SANDIA REPORT

SAND2016-0271
Unlimited Release
Printed January 2016

Verification of Advective Bar Elements Implemented in the Aria Thermal Response Code

Brantley H. Mills

Prepared by
Sandia National Laboratories
Albuquerque, New Mexico 87185 and Livermore, California 94550

Sandia National Laboratories is a multi-program laboratory managed and operated by Sandia Corporation, a wholly owned subsidiary of Lockheed Martin Corporation, for the U.S. Department of Energy's National Nuclear Security Administration under contract DE-AC04-94AL85000.

Issued by Sandia National Laboratories, operated for the United States Department of Energy by Sandia Corporation.

Available to DOE and DOE contractors from
U.S. Department of Energy
Office of Scientific and Technical Information
P.O. Box 62
Oak Ridge, TN 37831

Telephone: (865) 576-8401
Facsimile: (865) 576-5728
E-Mail: reports@osti.gov
Online ordering: http://www.osti.gov/scitech

Available to the public from
U.S. Department of Commerce
National Technical Information Service
5301 Shawnee Rd
Alexandria, VA 22312

Telephone: (800) 553-6847
Facsimile: (703) 605-6900
E-Mail: orders@ntis.gov
Online order: http://www.ntis.gov/search

SAND2016-0271
Unlimited Release
Printed January 2016

Verification of Advective Bar Elements Implemented in the Aria Thermal Response Code

Brantley H. Mills

Thermal Sciences and Engineering Department
Sandia National Laboratories
P.O. Box 5800
Albuquerque, NM 87185-MS0825

Abstract

A verification effort was undertaken to evaluate the implementation of the new advective bar capability in the Aria thermal response code. Several approaches to the verification process were taken: a mesh refinement study to demonstrate solution convergence in the fluid and the solid, visually examining the mapping of the advective bar element nodes to the surrounding surfaces, and a comparison of solutions produced using the advective bars for simple geometries with solutions from commercial CFD software. The mesh refinement study has shown solution convergence for simple pipe flow in both temperature and velocity. Guidelines were provided to achieve appropriate meshes between the advective bar elements and the surrounding volume. Simulations of pipe flow using advective bars elements in Aria have been compared to simulations using the commercial CFD software ANSYS Fluent® and provided comparable solutions in temperature and velocity supporting proper implementation of the new capability.

Acknowledgements

A special thanks goes to Dean Dobranich for his guidance and expertise through all stages of this effort. His advice and feedback was instrumental to its completion. Thanks also goes to Sam Subia and Tolu Okusanya for helping to plan many of the verification activities performed in this document. Thank you to Sam, Justin Lamb and Victor Brunini for their assistance in resolving issues encountered with running the advective bar element model. Finally, thanks goes to Dean, Sam, and Adam Hetzler for reviewing the document and providing very valuable comments.

Contents

Figures

Tables

Introduction

Aria is a finite element multi-mechanics module based on the Sierra Mechanics framework for solving coupled PDEs at Sandia National Laboratories. Aria developers have incorporated a new capability for modeling the advection of energy associated with fluid flow coupled convectively to a conductive solid body. In this model, fluids flowing internally through solid volumes are represented with a reduced order model using 1D bar elements that are thermally coupled to the surrounding 3D solid using empirical heat transfer coefficient (HTC) correlations. The primary advantage of this method is that relevant fluid flows can be integrated in very large 3D system level models without a significant increase in setup or computation time.

Conventional techniques for incorporating convection heat transfer in 3D thermal models typically use an empirical HTC correlation for relevant geometries with a specified constant reference temperature and velocity. Alternatively, the 3D continuity, momentum, and energy conservation equations for fluid flow are coupled with the model if more accuracy is required. In circumstances where convection does not significantly affect the relevant temperature profiles in the solid volume, the former method may be sufficient for the analyst. Even if the convection is relevant, if the velocity and temperature of the flow does not change significantly through the solid, then an empirical HTC correlation with constant reference temperature may still be acceptable. However, for cases where the solution is strongly influenced by convection and the fluid temperature can change considerably as the flow travels over the solid, coupling a model of the flow itself may be required.

Coupling the continuity, momentum, and energy conservation equations will likely yield the most accurate results if properly implemented, but the time it takes to apply and execute a 3D model of the fluid flow will be significant. Above all, in practical applications the additional accuracy from a 3D fluid simulation may not be worth the added setup (including meshing of the fluid volume) and computation time. This is especially true if the temperature and velocity of the fluid only change significantly in the direction of the fluid flow. In such cases, a 1D fluid model may be sufficient as is discussed in this document. The mass, momentum, and energy conservation equations that govern a 1D flow system are as follows:

$$\frac{\partial \rho}{\partial t} + \frac{\partial (\rho w)}{\partial z} = 0\,, \tag{1}$$

$$\rho \frac{\partial w}{\partial t} + \rho w \frac{\partial w}{\partial z} = -\frac{\partial p}{\partial z} + \frac{\partial \tau_{zz}}{\partial z}\,, \tag{2}$$

$$\rho c_v \frac{\partial T}{\partial t} + c_p \frac{\partial (\rho w T)}{\partial z} - \frac{\partial}{\partial z}\left(k \frac{\partial T}{\partial z} \right) = S \tag{3}$$

where ρ is the fluid density, z is the spatial coordinate in the flow direction, w is the fluid velocity, τ_{zz} is the viscous stress, S is a source term, T is the fluid temperature, c_v is the constant volume specific heat, c_p is the constant pressure specific heat, and k is the fluid thermal conductivity, p is the pressure. For a limited class of problems in which changes of fluid momentum are small and when there are negligible local changes of density with time, the net effect of solving Eqs. 1 and 2 can be captured using simply the steady term of Eq. 1. At the time of this document, this is the current implementation of the advective bar element model in Aria. Implicit in this current model is the ability to evaluate the density over a limited range of pressure. Future work will include modeling of all three conservations equations in their form presented in Eqs. 1-3.

The conservation equations are discretized using the finite element method, and 1D bar elements model the fluid volume. The 1D fluid bar elements are coupled to the surrounding 3D volume through a convection boundary condition on the surrounding solid. That is, the fluid temperature at each bar node is used as the reference temperature in Newton's Law of Cooling along with an appropriate empirical heat transfer coefficient (HTC) correlation on the surfaces nearest to that bar node. Additionally, the fluid velocity at a bar node is also used to calculate the Reynolds number at the surface nearest to the node for the HTC correlation. The advantage of this method (as opposed to specifying a constant reference temperature and velocity over the entire surface) is that it allows for the HTC correlations to be more accurately evaluated locally as the fluid temperature changes through the volume. In Aria, those correlations may be chosen from an extensive library already integrated in the code for both laminar and turbulent flow. Correlations are also available for free convection as well. Furthermore, with large changes in temperature, temperature dependent properties can be reevaluated.

This 1D fluid flow model, referred to as the 'advective bar' model here for brevity since it includes advection in the energy equation for the bar elements, has already seen use at SNL.[1,2,3] This speaks towards the model's utility, but it also emphasizes the need to evaluate the new model's implementation into Aria. The work provided in this document aims to support that effort.

The advective bar model underwent various verification activities to support the model's implementation into Aria. First, a mesh resolution analysis was performed to demonstrate convergent solution behavior as the mesh is

---

[1] Dobranich, D., "Ther2 Qualification Activity—Test-Design Simulation Support," SAND2014-17390, September 2014.

[2] Dobranich, D., Hetzler, A., Francis, N. "Ther2-WR Qualification Activity—Model Validation Evidence in Support of Environmental Specifications," SAND2015-9654, November 2015.

[3] Dobranich, D., Mills, B., "Ther2-JTA Qualification Activity – Model Validation Evidence," Draft SAND Report

uniformly refined. Next, a series of meshes with different varying element sizes in the streamwise direction were visually inspected to determine if the nodes on the fluid elements are being properly mapped to the surrounding solid volume. Finally, solutions from a widely utilized CFD commercial software program, ANSYS Fluent®, were compared to the solutions from Aria using advective bars for simple geometries. Future efforts should continue to expand upon and complement the work provided in this document.

Introduction

Advective Bars in the Literature

Using the finite element method to discretize the 1D mass, momentum, and energy conservation equations for fluid flow is often cited in textbooks on the subject for illustration of the method.[4] Seldom is a 1D fluid flow model used on its own in practice today with ample computational power available to analysts. However, there are problems in which using a reduced order model, like for 1D fluid flow, coupled with dimensionally higher-order models may provide approximate solutions that are within an acceptable range of uncertainty (within the uncertainty of any experimental measurements). Often the validity of certain assumptions that may need to be made to computationally solve dimensionally higher-order models (*e.g.* turbulence models) bolsters the appeal of a reduced order model. The application of these approaches is often left at the analyst's discretion.

The advective bar model that has been implemented in Aria discussed in this document is a 1D fluid flow model (including the mass, momentum, and energy conservation equations) with the capability to be thermally coupled with a 3D finite element model to represent internal fluid flow (the model can also be extended to model external flow). The advantage of this model, is that is provides analysts the ability to integrate a computationally inexpensive model of internal fluid flow convectively coupled to complex system level models. Without this approach, analysts may typically be required to specify a constant heat transfer coefficient on the respective surface (typically from an empirical correlation for an appropriate geometry) and a constant reference temperature. While this may provide an acceptable answer, when abrupt changes in temperature occur in the streamwise direction, significant error can be introduced into the surrounding 3D volume. One alternative to capture this effect is to model the entire 3D fluid volume, but this is typically computationally expensive and may require a significant amount of effort to appropriately mesh. For unidirectional flow, the additional accuracy of a 3D fluid model may not warrant the additional effort and time. Thus, the advective bar model provides a compromise between these two extremes.

A computer program was developed at Sandia National Laboratories (SNL) in the early 90s named SAFSIM[5] (System Analysis Flow Simulator) which served as the foundation of the advective bar model now implemented into Aria. SAFSIM was a FORTRAN computer program used to model the fluid mechanics, structure heat transfer, and reactor dynamics of a flow system. The goal of SAFSIM was to provide quick and inexpensive investigation into steady-state and transient behavior of systems that may include complex interactions

---

[4] Reddy, J. "An Introduction to the Finite Element Method", McGraw-Hill, 3rd Edition, New York, New York (2006)

[5] Dobranich, D., "SAFSIM Theory Manual – A Computer Program for the Engineering Simulation of Flow Systems", SAND92-0693, Printed November 1993

and feedback mechanisms during normal and off-normal conditions. An 'engineering approach' was applied in the program to enable analysts to approximate solutions to complex system level flow problems quickly. As part of that approach, a 1D finite element model was implemented for fluid flow. While SAFSIM also provided analysis beyond heat transfer (including species transport), the basic fluid model using 1D bar elements was the basis for the model that has been implemented into Aria.

Few examples of 1D fluid flow thermally coupled to 3D models for improved modeling of convective heat transfer were found in the literature outside of SNL. However, 1D fluid flow models can be found integrated in some well-known software programs. One example of such a software program that is used for transient thermal hydraulic analysis of light water nuclear reactors is RETRAN-02. It utilizes a 1D homogeneous equilibrium mixture model for two phase fluid flow that can model heat transfer between systems in the coolant loop.[6] Outside of heat transfer, 1D fluid flow networks have also been regularly used in biological applications to model blood flow in arteries and veins.[7,8] Other finite element packages, such as LS-DYNA,[9] have implemented boundary elements to model fluid flow over a surface (2D), but without a focus of heat transfer to the solid.

Some recent examples of 1D fluid flow thermally coupled with 2D or 3D bodies were found in the literature with applications in modeling geothermal heat transfer.[10,11] In both of these examples provided here, the fluid models were thermally coupled to the surrounding volumes (in these examples large bodies of soil) through convection boundary conditions. In addition, both models utilized empirical turbulent heat transfer coefficient correlations when appropriate. Conduction radially through the piping housing the fluid flow was included as an additional resistance in an effective HTC. Both examples used the finite element package COMSOL Multiphysics® as the framework for the model. As these models were custom implementations into COMSOL, no type of verification or validation of the models has been performed.

---

[6] CSA Inc., RETRAN-02. *CSA: Nuclear Power Industry Engineering & Consulting.* [Online] http://www.csai.com/retran/R02index.html.

[7] Barnard, W., et al., "A Theory of Fluid Flow in Compliant Tubes," Biophysical Journal, 6, 717-724 (1966)

[8] Sochi, T., "One-Dimensional Navier-Stokes Finite Element Flow Model", Technical Report, April 9, 2013

[9] LS-DYNA Dev, "LS-DYNA® Theory Manual," Livermore Software Technology Corporation, r:6702, August 11, 2015

[10] Saeid, S., et al., "An efficient computational model for deep low enthalpy geothermal systems," Computers & Geosciences, 51, 400-409 (2013)

[11] Ozudogru, T., et al., "3D numerical modeling of vertical geothermal heat exchangers," Geothermics, 51, 312-324 (2014)

Mesh Refinement Study

As part of the verification effort for the implementation of the advective bar elements into Aria, a mesh refinement study was performed. The goal of this study was to assure that solution convergence was observed in the temperature and velocity in both the pipe and the fluid as the mesh was uniformly refined. A series of simulations were performed on a simple geometry with progressively finer meshes using constant material properties. The simulations were then repeated using temperature dependent material properties. The local values for temperature in both the pipe and the fluid were also used to calculate the observed order of accuracy (*i.e.* the rate at which the discretization error is reduced as the mesh is refined)[12] to determine if the order matched the theoretical rate.

The problem chosen for the mesh refinement study was simple pipe flow. The parameters of this problem were also used later in this document for analyzing the mapping of the bar elements to the surrounding surfaces and for comparison with commercial CFD software. The geometry is depicted in Figure 1.

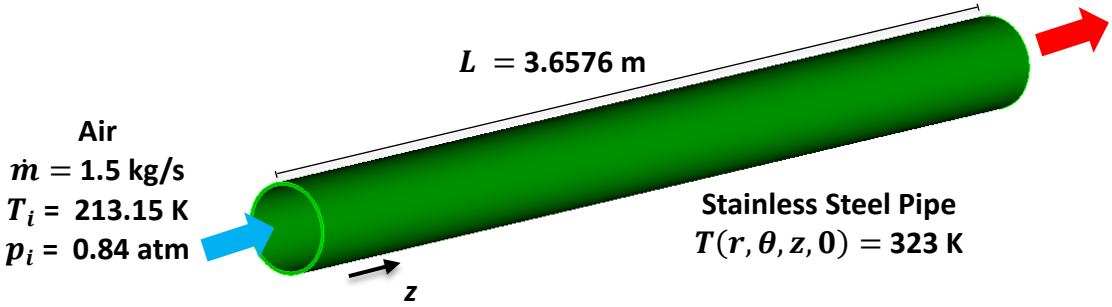

Figure 1. Diagram of the pipe flow geometry used in the mesh refinement study

In this problem, air at a mass flow rate $\dot{m}$ of 1.5 kg/s, inlet temperature T_i of 213.15 K, and inlet pressure p_i of 0.84 atm (85.11 kPa) flowed through a stainless steel pipe at an initial temperature $T(r,\theta,z,0)$ of 323 K. The pipe length L was 3.6576 m and has an inner diameter D_i and outer diameter D_o of 0.28 m and 0.3 m, respectively. Adiabatic boundary conditions were applied on the outer surface of the pipe and at the entrance and exit to the pipe. Convective heat transfer occurred on the inside surface of the pipe from the flowing air. The relevant output from the simulation for this problem included the outside temperature of the pipe wall, the average temperature of the air, and the average velocity of the air over the 2400 s.

[12] Oberkampf, W. L., and Roy, C. J., Verification and Validation in Scientific Computing, Cambridge University Press, New York, 2010.

Mesh Refinement Study

Given the simplicity of the geometry for this analysis, five uniformly refined meshes were created using hexahedral elements in the pipe and bar elements for the air. The coarsest mesh contained 10 elements along the length of the pipe and around its circumference. Five bar elements were used for the fluid for a total of 105 elements (100 hexahedral elements and 5 bar elements). This mesh was uniformly refined by decreasing the element dimensions by a factor of two resulting in eight times more elements (in the 3D volume) per refinement. The mesh refinement was performed four times to generate the other four meshes. The most refined mesh contained 409680 elements (409680 hexahedral elements and 80 bar elements). The time step used in the simulation for each refined mesh was halved starting with a value of 1 s for the coarsest mesh.

Although Aria has the capability to implement empirical heat transfer coefficient correlations into the advective bar problem, they were omitted for this mesh refinement study. A constant HTC of 45 W/m^2K was used. This value was an approximate value for the conditions depicted in Figure 1 as calculated from the Gnielinski correlation for circular pipe flow with air.[13] As previously stated, constant material properties were used for both the air and the pipe. The reason for a constant heat transfer coefficient and constant material properties was to simplify the problem for calculating the order of accuracy locally across the pipe. Temperature dependent properties were included later to evaluate their effect. Using constant material properties for the fluid simplified the problem and the resulting constant velocity V for the air could be calculated simply by

$$V = \frac{\dot{m}}{\rho A} \tag{4}$$

where $A = 6.1575\times10^{-2}$ m^2 was the cross sectional area of the pipe.

Figure 2 and Figure 3 present the exit air temperature and the exit wall temperature on the outside of the pipe (temperature profile on the pipe is axisymmetric), respectively. The numbers in the legend indicate the number of hexahedral elements in the pipe in the flow direction for each of the five meshes (the coarsest mesh contained 10 elements in the streamwise direction whereas the most refined mesh contained 160 elements). Even for the coarsest mesh with only 100 elements in the pipe and 5 bar elements for the fluid, the exit air temperature deviated from the most refined mesh with 409,600 elements in the pipe and 80 elements for the fluid, by a maximum of 0.4ºC. Likewise, for the exit wall temperature, the maximum difference between the coarsest mesh and the most refined mesh was 1ºC. Based on the scale of the temperature change in this problem, the model was relatively insensitive to the

[13] Gnielinski, V., "New equations for heat and mass transfer in turbulent pipe and channel flow," International Chemical Engineering, Vol. 16, No. 2, 359-367 (1976).

mesh resolution. In addition, both temperature profiles were observed to converge as the mesh was refined.

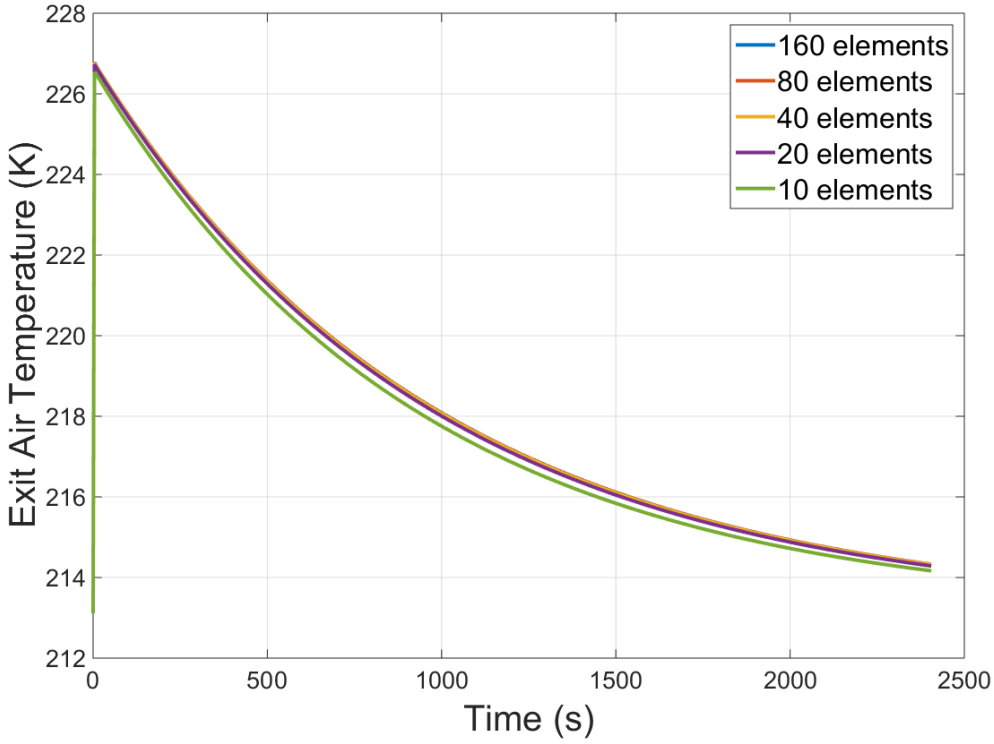

Figure 2. Exit air temperature profiles with time for the five uniformly refined meshes

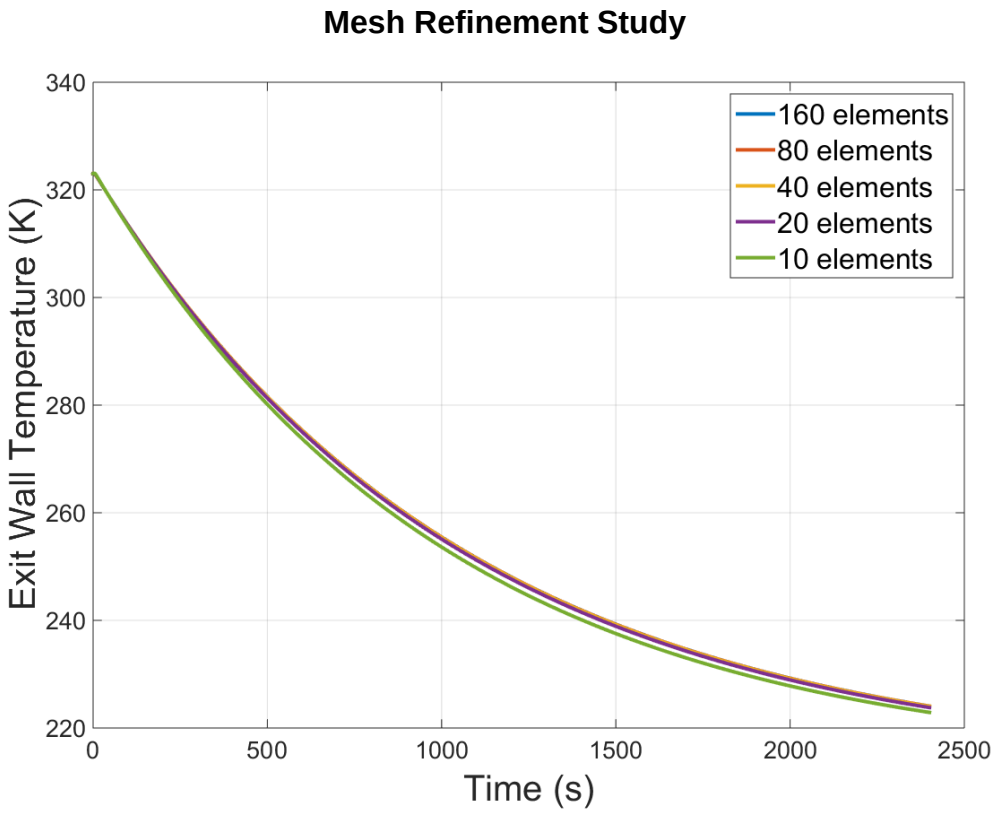

Figure 3. Exit wall temperature profiles with time for the five uniformly refined meshes

The temperature profile along the length of the pipe at 11 equally spaced locations in the fluid and the pipe (only 6 locations in the coarsest mesh for the fluid) at t = 2400 s is plotted in Figure 4 and Figure 5, respectively. Each location corresponds to a node along the length of the pipe. Differences between the most refined mesh and the coarsest mesh were more evident when plotting the temperature profile along the length of the pipe as the scale was smaller in the figures. Again, both temperature profiles were observed to converge as the mesh was refined.

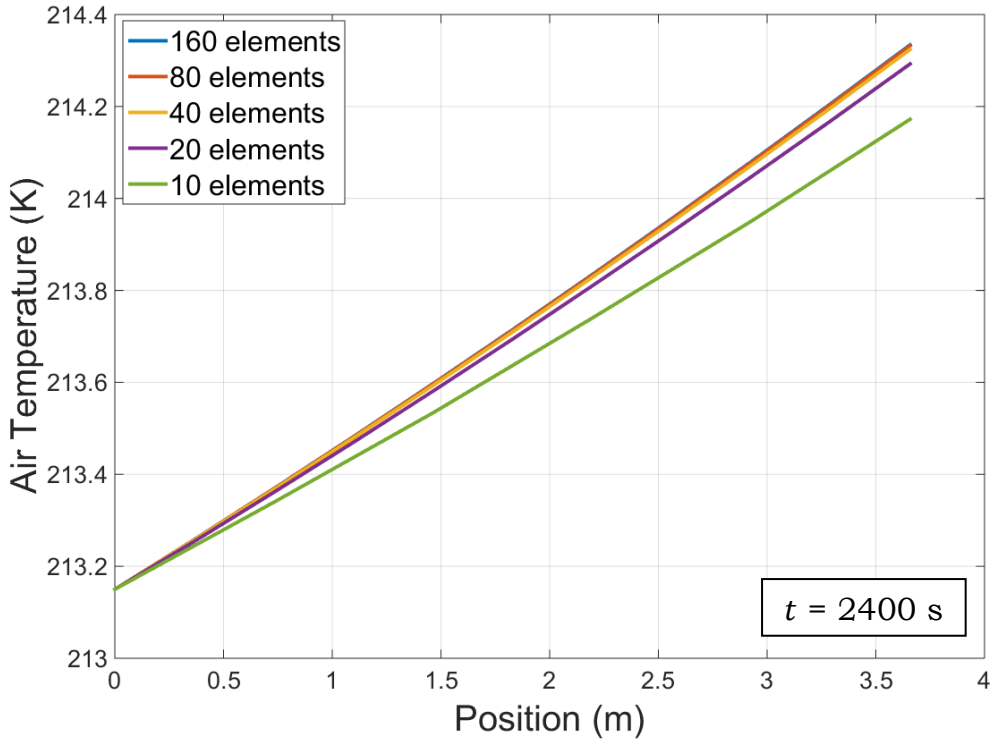

Figure 4. Air temperature profiles along the length of the pipe for the five uniformly refined meshes at t = 2400 s

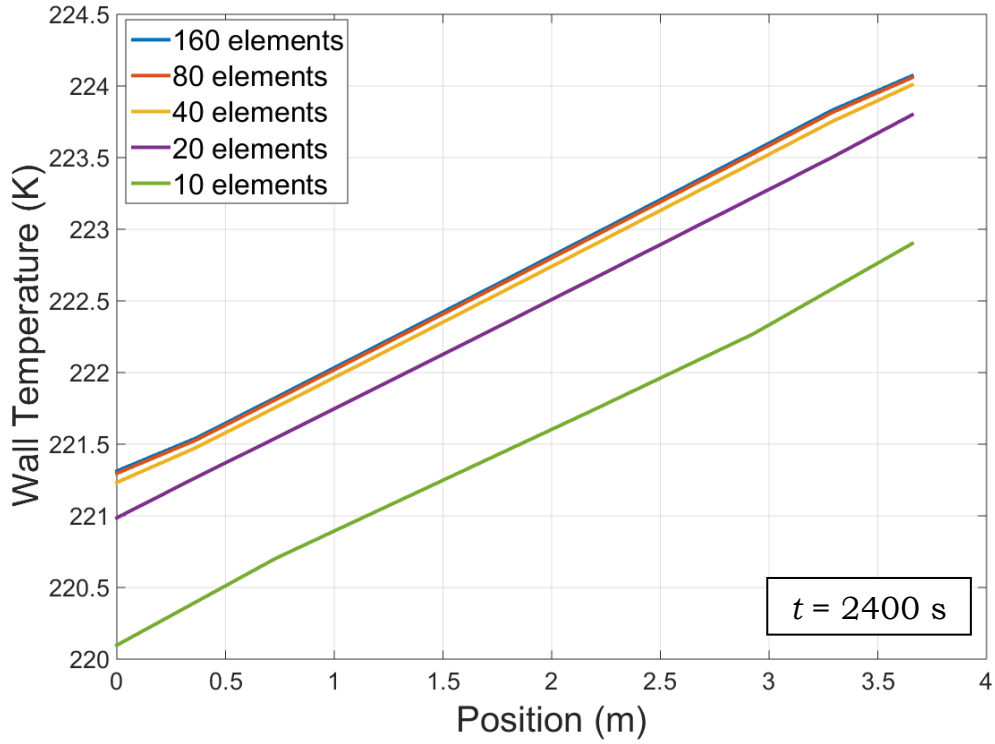

Figure 5. Wall temperature profiles along the length of the pipe for the five uniformly refined meshes at t = 2400 s

The converging behavior is more clearly observed by plotting the exit air temperature and exit pipe temperature at t = 2400 s as a function of the axial element size in Figure 6 and Figure 7, respectively. In both figures, the temperature asymptotically approached a value with the change in the temperature steadily decreasing as the mesh was refined. The observed order of accuracy $\hat{p}$ was calculated using three of the meshes for air temperature and the pipe wall temperatures distributed locally along the length of the pipe

$$\hat{p} = \frac{\ln\left(\frac{T_3 - T_2}{T_2 - T_1}\right)}{\ln(2)} \tag{5}$$

where T_i is the temperature at a given location on the ith mesh (3 referred to the coarsest mesh and 1 referred to the most refined mesh of the three meshes). The results of the calculation are shown in Figure 8 and Figure 9 for the air temperature and the pipe wall temperature, respectively. As the mesh is refined, the observed order of accuracy for both temperatures approaches a value of two locally. The discretization scheme for the solid volume was second order in both space and time, and the observed order of accuracy converged on this value of two throughout the pipe in Figure 9.

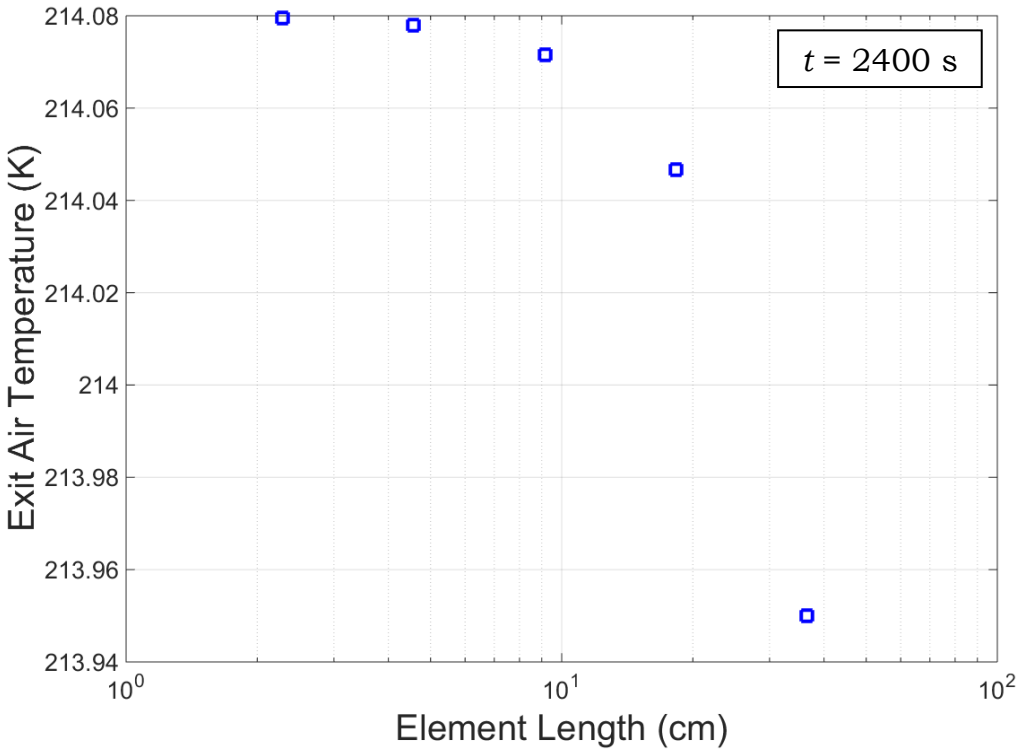

Figure 6. Exit air temperature at t = 2400 s versus the axial element size

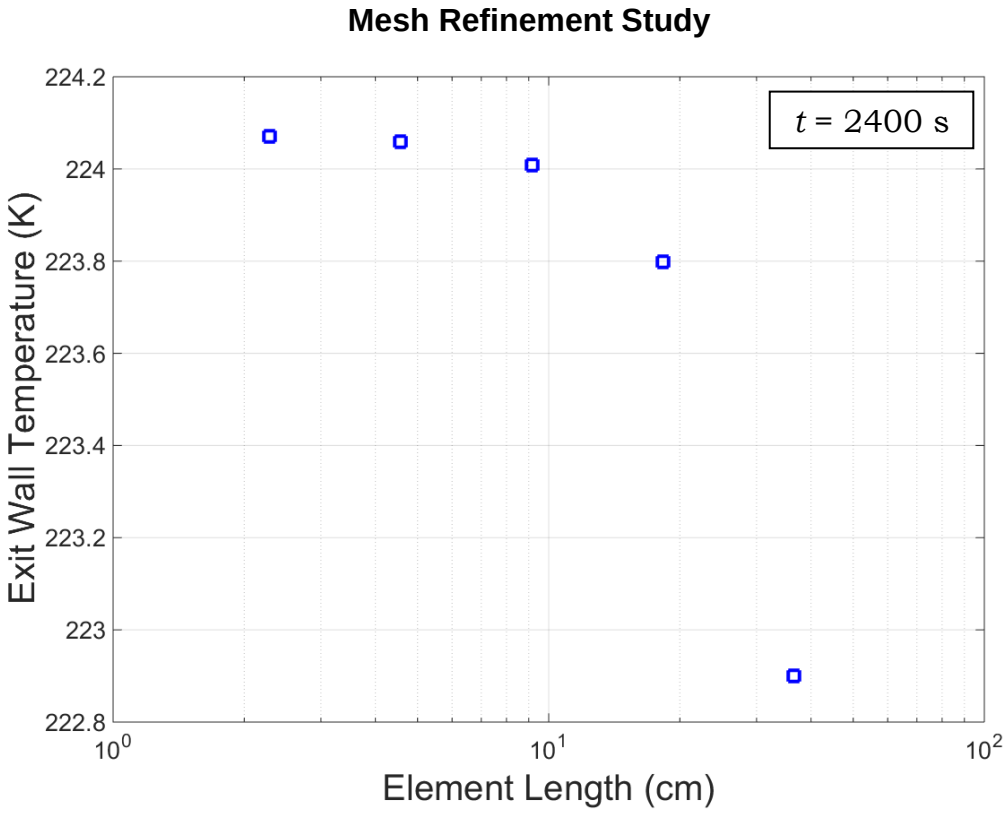

Figure 7. Exit wall temperature at t = 2400 s versus the axial element size

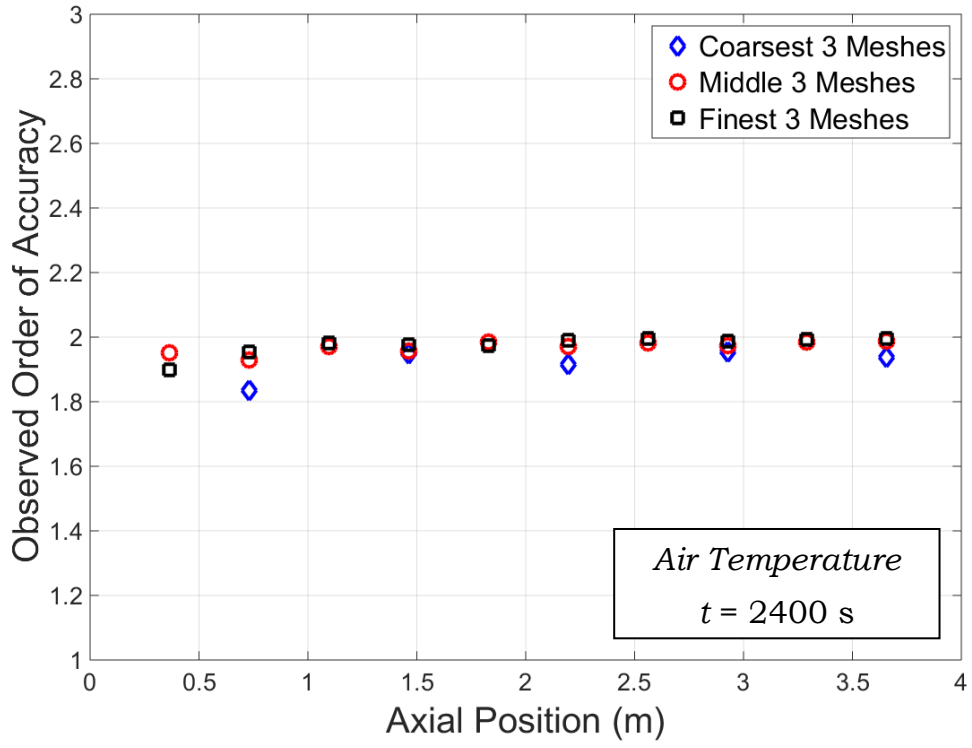

Figure 8. Observed order of accuracy for the local air temperature at t = 2400 s calculated from the five uniformly refined meshes

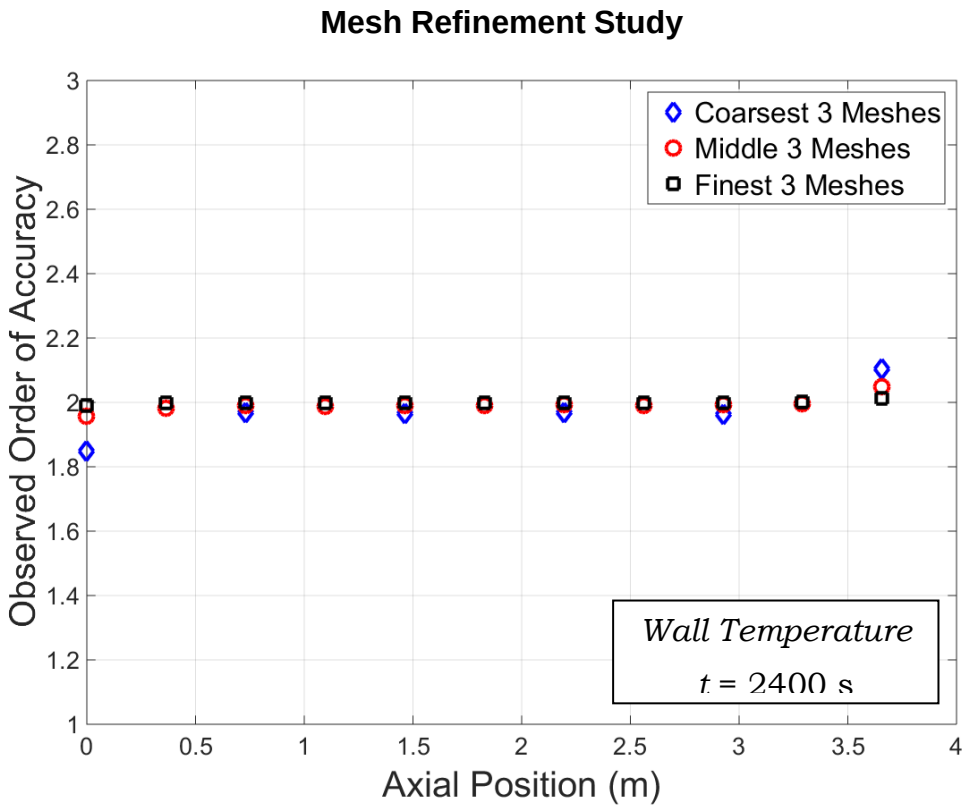

Figure 9. Observed order of accuracy for the local wall temperature at t = 2400 s calculated from the five uniformly refined meshes

The simulations were repeated using temperature-dependent material properties in both the fluid and the pipe. Including temperature dependent properties in the fluid created a non-constant fluid velocity along the length of the pipe (resulting from changes in the fluid density). Temperature-dependent properties used in this example are provided in Appendix A. The solution for the exit temperature in the fluid and pipe are provided in Figure 10 and Figure 11, respectively, and the solution for fluid velocity is provided in Figure 12. As with the case with constant material properties, the temperatures and velocity were observed to converge with increasing mesh resolution. However, unlike the previous simulations, the temperature deviated by up to 2°C in the air temperature between the coarsest and most refined mesh. For the exit velocity, the largest difference throughout the profile was 0.15 m/s.

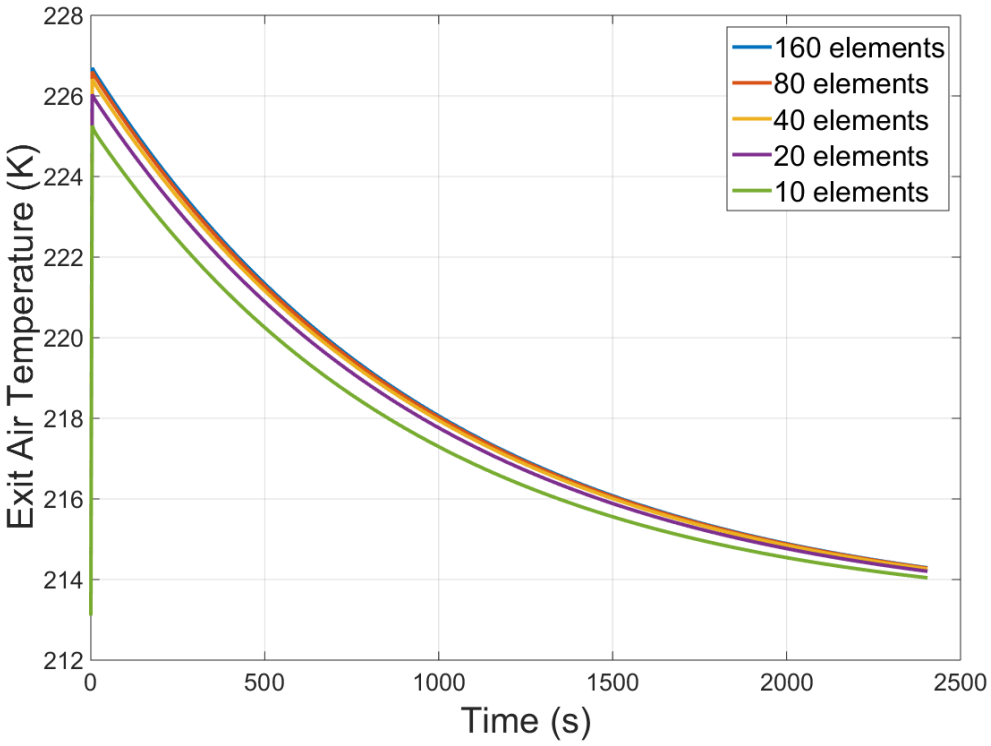

Figure 10. Exit air temperature profiles with time for the five uniformly refined meshes

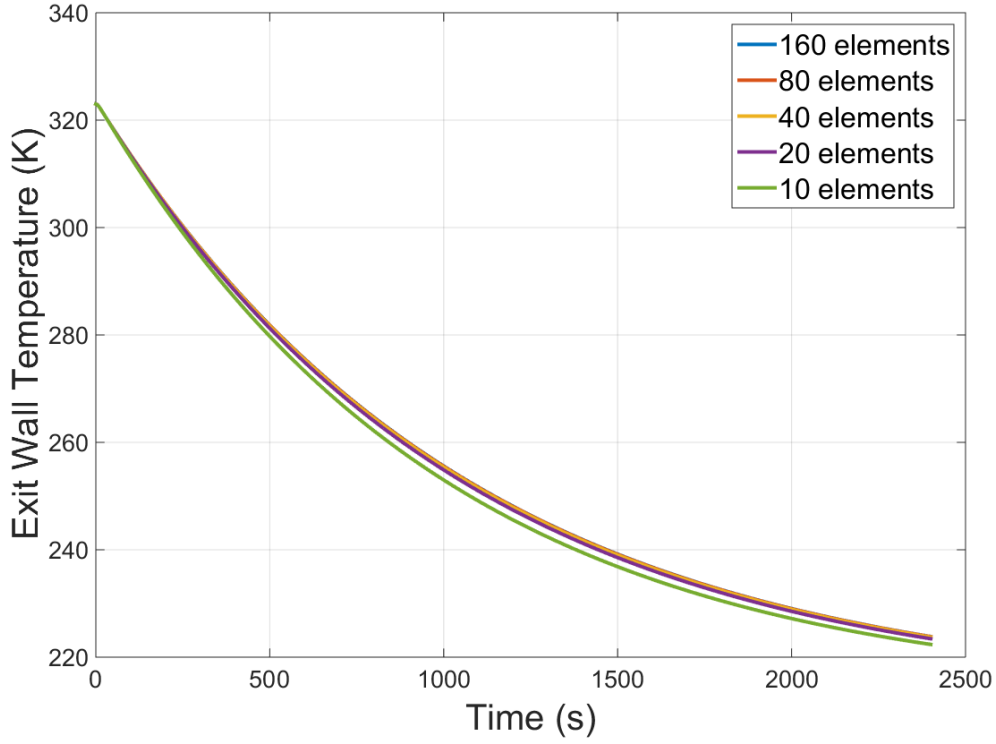

Figure 11. Exit wall temperature profiles with time for the five uniformly refined meshes

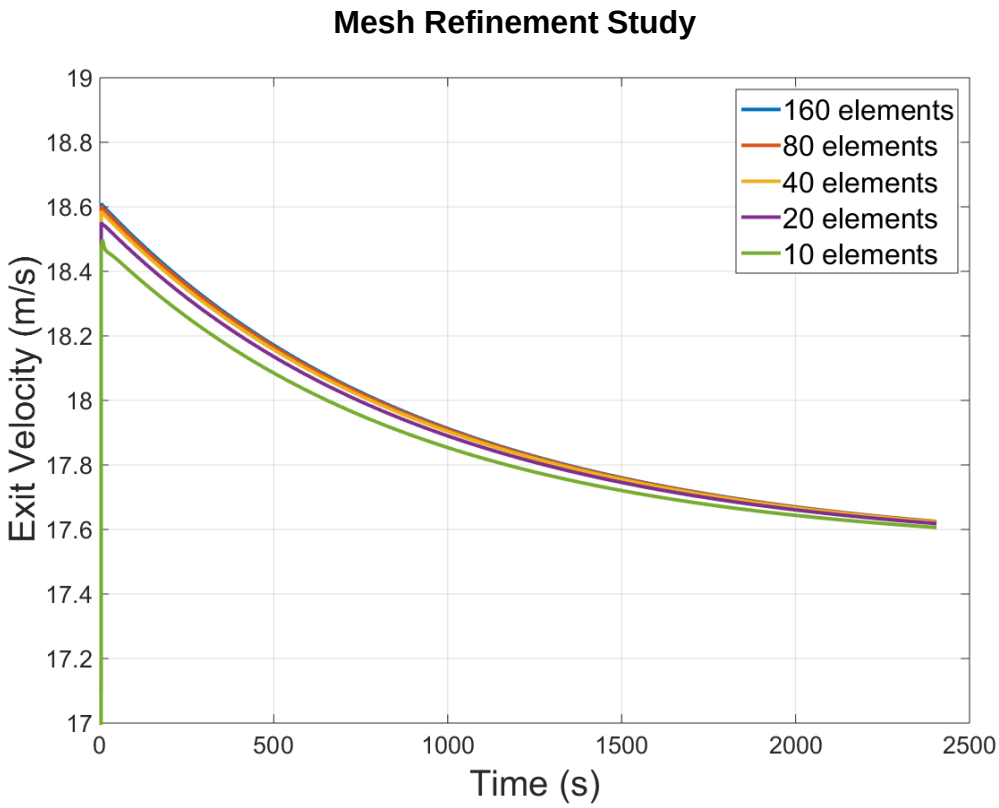

Figure 12. Exit air velocity profiles with time for the five uniformly refined meshes

The observed order of accuracy was again calculated along the length of the pipe using Eq. 5 with the three most refined meshes for the temperature in the fluid, the wall temperature in the pipe, and the velocity in the fluid. This is presented in Figure 13. As in Figure 9, the wall temperature converges with an order of two as expected. However, the fluid temperature, which also was previously observed to converge with an order of two in Figure 8, converged with an order of approximately three as the mesh was refined. Further order of accuracy tests investigating the order of convergence with an exact solution should be performed on the bar elements for this problem evaluating properties such as L2 Norms as opposed to local responses.

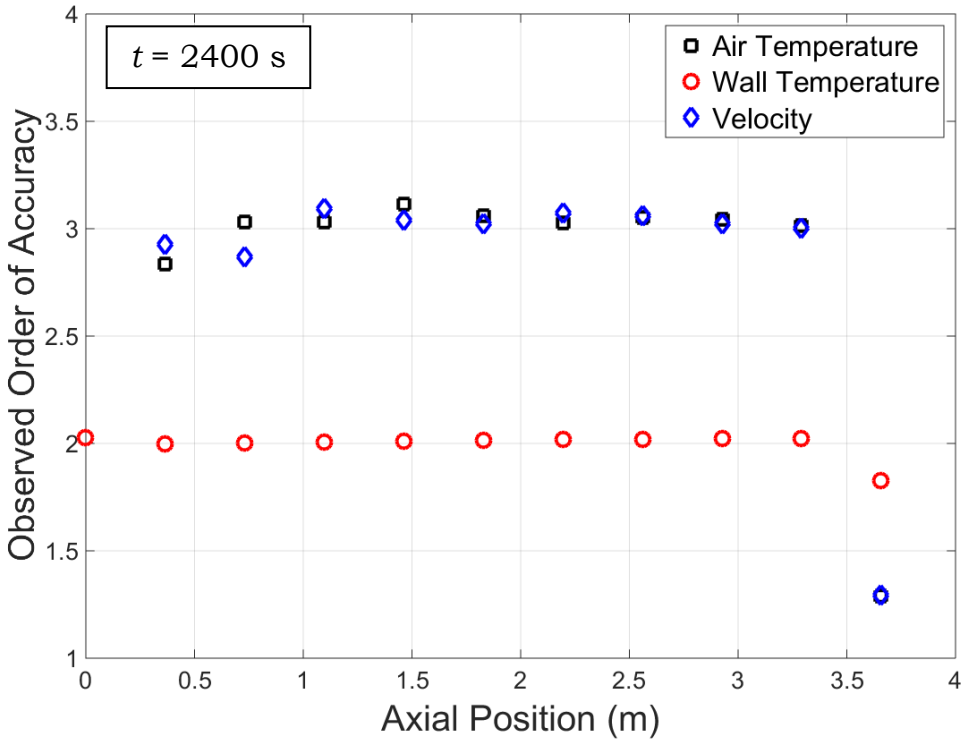

Figure 13. Observed order of accuracy for fluid temperature, wall temperature, and fluid velocity at t = 2400 s for the three most refined meshes using temperature dependent properties

Mesh Refinement Study

Streamwise Mesh Mapping

Advective bar elements that are used with 3D finite element models require accurate mapping of nodes from the bar elements to the internal surfaces of the surrounding volume. This mapping is based upon the minimum distance from the centroid of surrounding surface elements to a bar node and provides the only means by which the 1D fluid model is coupled with the 3D solid model. Specifically, it defines the fluid temperature used as the reference temperature in the convection boundary condition on the surrounding surfaces. When a heat transfer coefficient correlation model is included, it also defines the local velocity of the fluid used in the calculation of the heat transfer coefficient, which is used in the calculation of the local Reynolds number.

This study specifically investigated axisymmetric geometries such as pipe flow and annular flow that would have favorable characteristics for use with advective bar elements (*i.e.* unidirectional flow). While the model was not limited to these simple geometries, using them for the analysis in this document reduced the complexity of the fluid flow. In both pipe flow and annular flow, the advective bar elements were defined along the axis of the pipe. In annular flow this meant the elements were obscured by the inner cylindrical volume. This study explored how the nodes on the bar elements were mapped for varying element lengths in the streamwise direction where a large change in temperature and velocity may be observed in the flow. In practical applications using complex system models, it may prove difficult or impractical to completely control the bar element size with respect to the surrounding surfaces in the streamwise direction.

Several meshes for pipe flow were visually inspected with varying mesh sizes between the surrounding volume and the bar elements to confirm the mapping was being properly performed. A visualization capability implemented in Aria that identified to which surfaces each node was mapped was used to evaluate each case. Guidelines are presented here that will aid in avoiding common problems that could arise in the meshing the bar elements.

A number of meshes were generated using the previous pipe flow problem described in the mesh resolution study (for a duration of 1200 s) with varying constant element lengths in the streamwise direction between the surrounding hexahedral pipe elements and the bar elements. Table 1 summarizes the cases that were investigated. Three primary cases were considered: an equal number of elements in the pipe and fluid axially, 160 bar elements axially with varying number of elements in the pipe from 10 to 80, and 160 elements in the pipe axially with varying number of bar elements from 10 to 80. One further case was considered where the nodes of the pipe and bar elements did not align for the entire length of the pipe.

Table 1. Summary of the Pipe Flow Meshes

Case #	# of Pipe Elements	# of Bar Elements
1	160	160
2	10	10
3	10	160
4	20	160
5	40	160
6	80	160
7	160	10
8	160	20
9	160	40
10	160	80
11	77	23

Using Aria's visualization capability, the meshes in Table 1 were visually inspected using CEI EnSight®. The results are summarized in Figure 14. For cases with 160 bar elements and 10 to 80 pipe elements (Figure 14a), the mapping between the pipe and bar elements occurred as expected. Bar nodes at the midpoint of each surface were mapped to the surrounding surfaces while the extra bar nodes were not mapped to any surface. For cases with 160 pipe elements and 10 to 80 bar elements (Figure 14b), the mapping between the pipe and bar elements also occurred as expected. Surfaces were equally split between two adjacent bar nodes with bar nodes at the ends getting half as many surfaces as interior nodes. For an equal number of pipe and bar elements (Figure 14c), the mapping between the elements became irregular. Since each surface was equally split between two nodes, it became difficult for Aria to properly assign each node to a surface consistently such that azimuthal variations in the mapping appeared. The effect from these variations decreased for an increasing number of elements; however, analysts should avoid such scenarios. Note that while the case in Figure 14c was not identified in Table 1, it was presented here for illustration of the common problem observed for an equal number of elements. For cases such as Figure 14d where the nodes between the fluid elements and elements in the pipe do not align, the mapping occurred as expected with some nodes covering a larger surface area of the pipe. This was most likely the scenario that would be encountered in practical applications where the number of elements in the surrounding volume may not match the fluid elements or even be regular. A small defect was observed in Figure 14d at the center of the pipe. This occurs for the same reason as observed in Figure 14c, where an odd number of elements in both the pipe and

the fluid (even number of nodes) created a surface in the center of the pipe that will be evenly split between two nodes. Such a defect would only be noticeable if there were a large temperature gradient in that location, but should be avoided if possible.

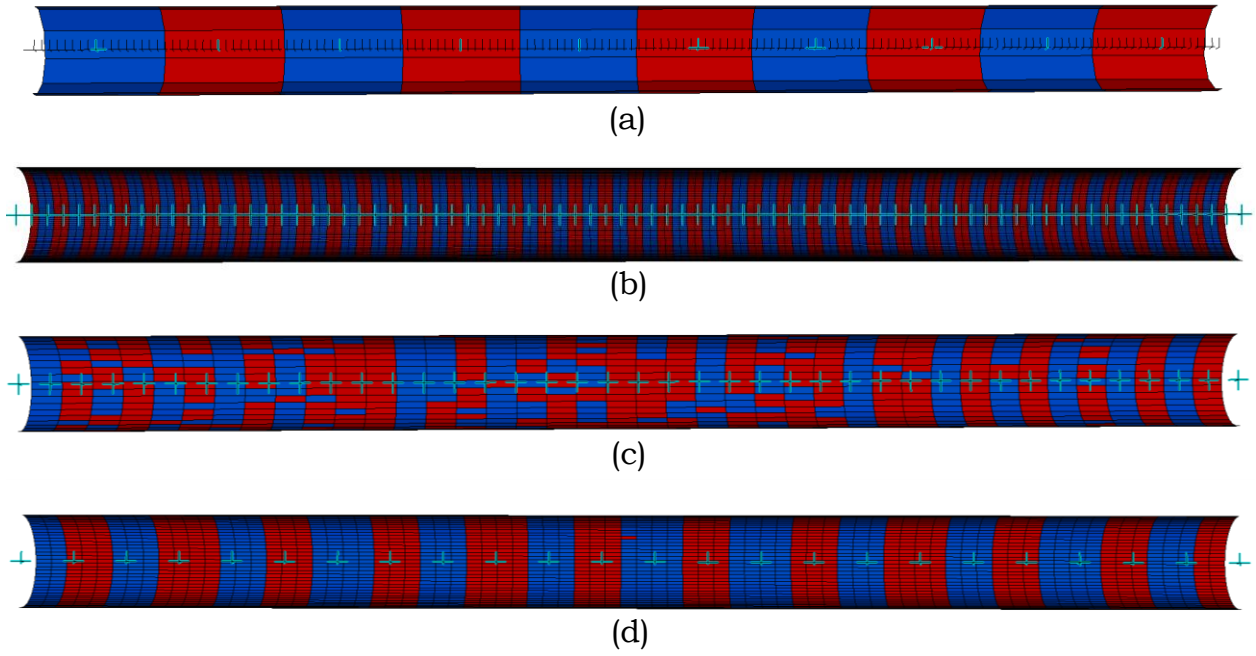

Figure 14. Graphical depictions of the mapping of bar nodes to the surrounding pipe surfaces for (a) 10 pipe elm., 160 bar elm., (b) 160 pipe elm., 80 bar elm., (c) 40 pipe elm., 40 bar elm., (d) 77 pipe elm., 23 bar elm. Highlighted nodes in the bar elements are the mapped nodes to their respective surfaces.

The temperature profile in the pipe and fluid and the velocity profile in the fluid at the exit of the pipe for each case are plotted with time in the following figures. The numbers in the legend indicate the number of elements in the pipe in the streamwise direction followed by the number of bar elements. In all the figures, it was observed that the mesh alignment did not have a significant impact on the final solution and the solution was converging for increasing mesh resolution. The case with 10 elements in the pipe and 10 bar elements (case 2 in Table 1) showed the largest deviation from the other solutions with higher resolution. In addition to having a low mesh resolution, this case also suffered from the effects observed in Figure 14c. However, as seen in the case with 160 elements in the pipe and 160 bar elements, this effect was less significant as the resolution increased and the solution was nearly identical to the solution with 160 elements in the pipe and 80 bar elements. It was also observed that the solutions with more bar elements than elements in the pipe axially converged on a slightly higher solution in both temperature and velocity. Although small, this effect could be a result of the differences in how the bar nodes were mapped to the surfaces (Figure 14a *vs.* Figure 14b). When

more elements in the pipe were used than bar elements, the last bar node was mapped to the last surface as opposed to the bar node in the middle of the surface. Therefore, the heat transfer that occurred between the final surface and the final bar node was smaller as a higher reference temperature for that surface was used for the boundary condition. This trend was reversed near the start of the pipe where a lower reference temperature was observed.

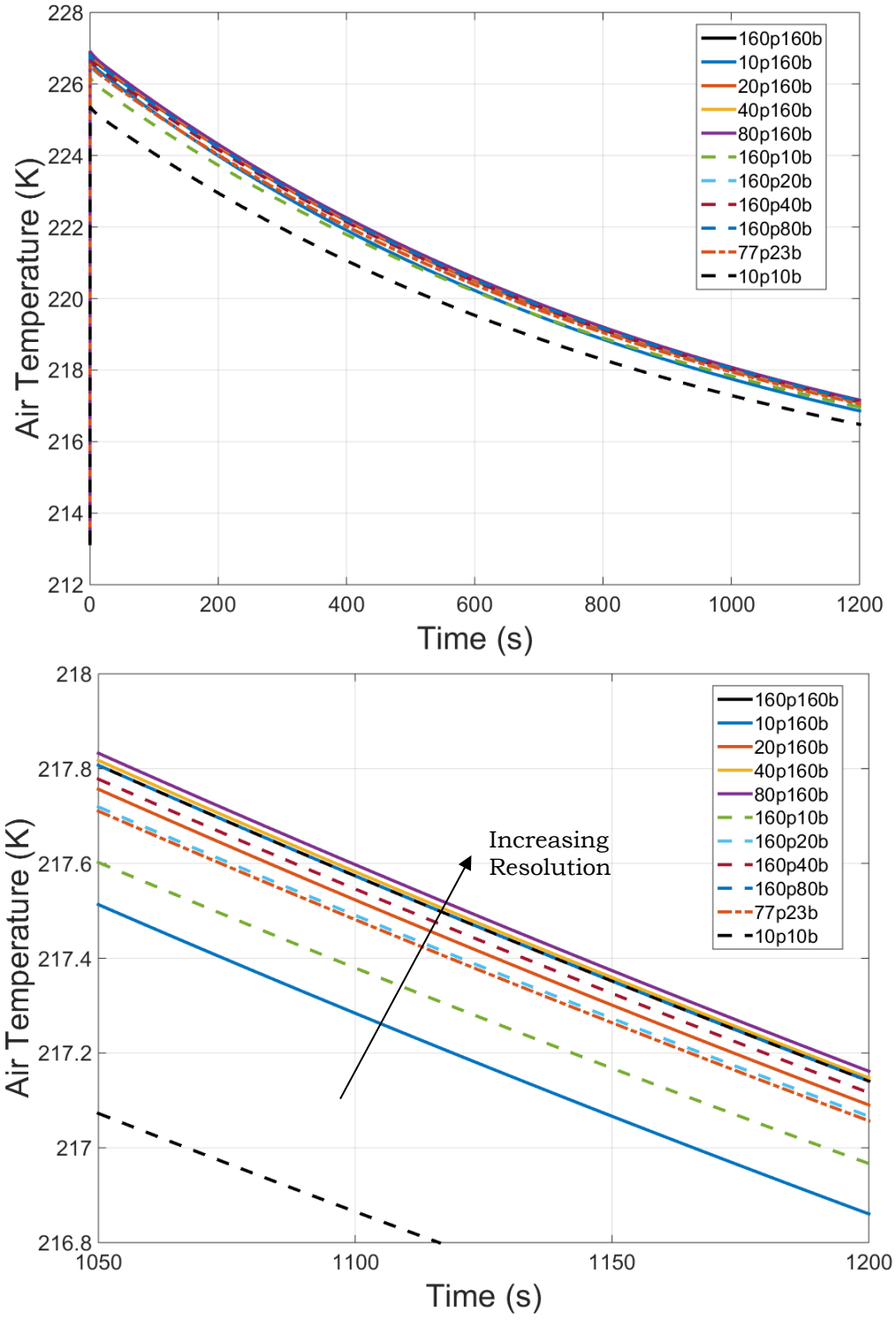

Figure 15. The air temperature profile for the entire time profile (top) and the last 150 seconds (bottom) at the pipe exit for all cases in Table 1.

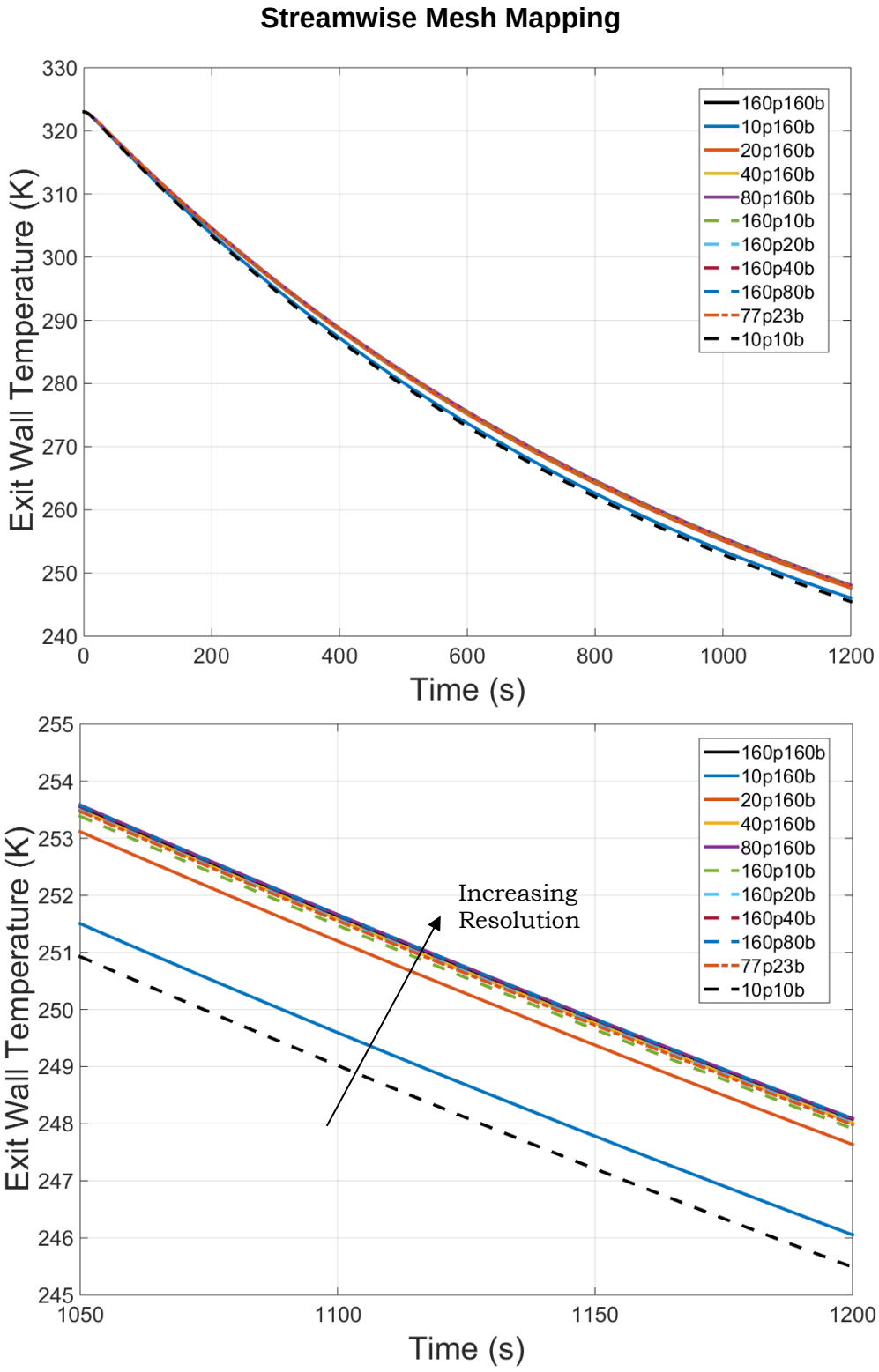

Figure 16. The wall temperature for the entire time profile (top) and the last 150 seconds (bottom) profile at the pipe exit for all cases in Table 1.

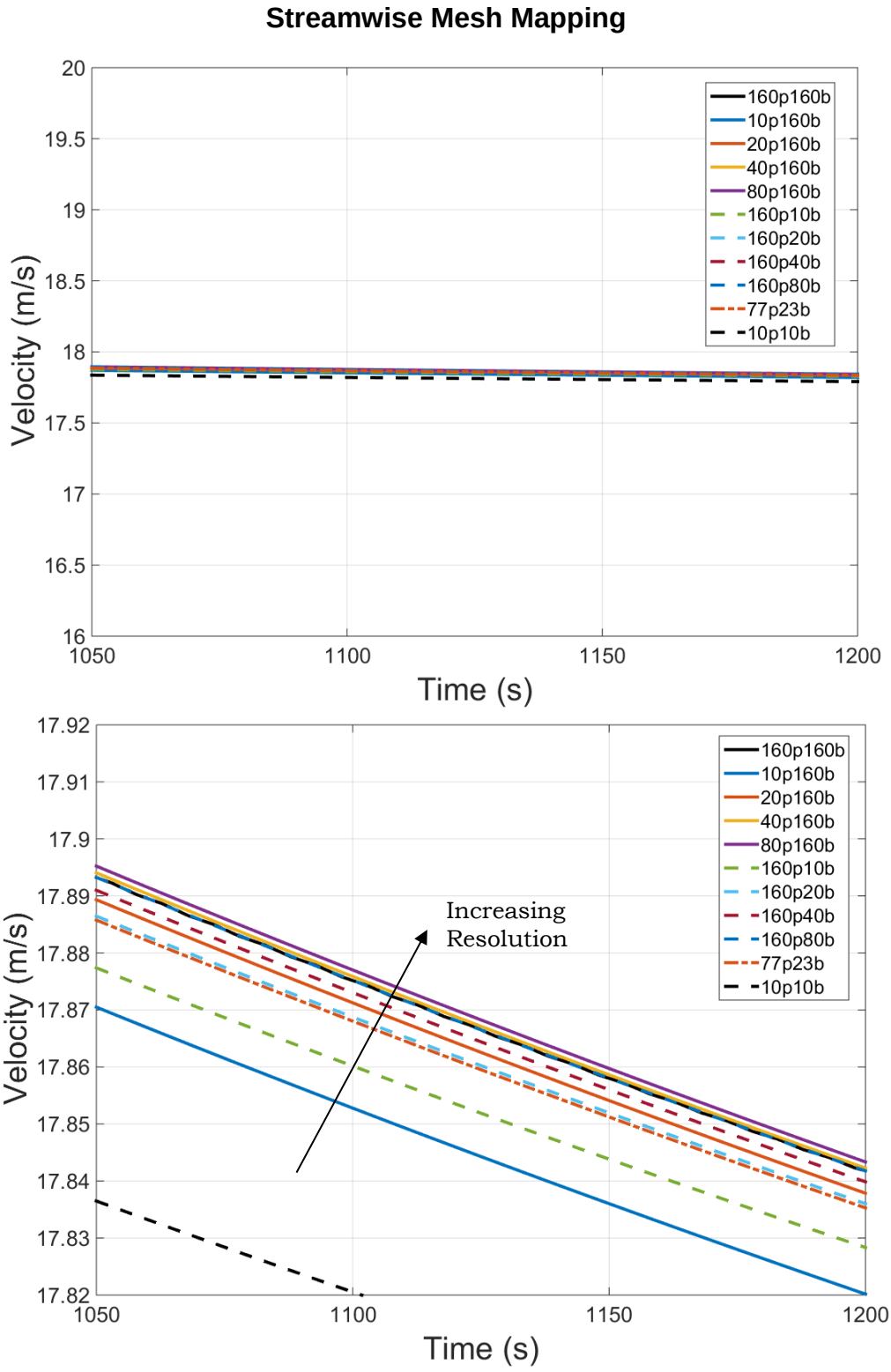

Figure 17. The velocity profile for the entire time profile (top) and the last 150 seconds (bottom) at the pipe exit for all cases in Table 1.

In all three of the previous figures, the temperature of the air was not heavily influenced by the number of elements in the streamwise direction. For practical applications, where a high resolution mesh would be applied to the

surrounding volume, very few bar nodes were required to approach a converged solution. The difference in the exit air temperature when using 10 bar elements versus 80 bar elements is less than 0.4°C. For the pipe exit temperature, the difference was less than 3°C. If large local fluctuations in convective heat transfer appeared in the streamwise direction, more bar elements in these regions would be required.

The following figures present the temperature of the fluid and the pipe and the velocity profile along the length of the pipe at t =1200 s. The numbers in the legend indicate the number of elements in the pipe followed by the number of bar elements in the streamwise direction. As shown in the figures, the streamwise mesh alignment did not significantly affect the temperature and velocity profiles with the exception of the coarsest meshes. For the mesh with 10 bar elements and 10 pipe elements, the profile was very irregular as a result from the effects observed in Figure 14c. For the mesh with 160 bar elements and 10 elements in the pipe, the temperature profiles were smooth but showed a relatively large deviation from the higher resolution meshes. For meshes with more elements in the pipe than bar elements, the air temperature and velocity profiles decreased at the end of the pipe. This was likely a result of the bar nodes at the end of the pipe being coupled to the surfaces at the pipe exit (Figure 14a *vs.* Figure 14b). Since adiabatic boundary conditions were applied at the ends of the pipe, the temperature profile exhibited temperature profiles without a gradient at each end.

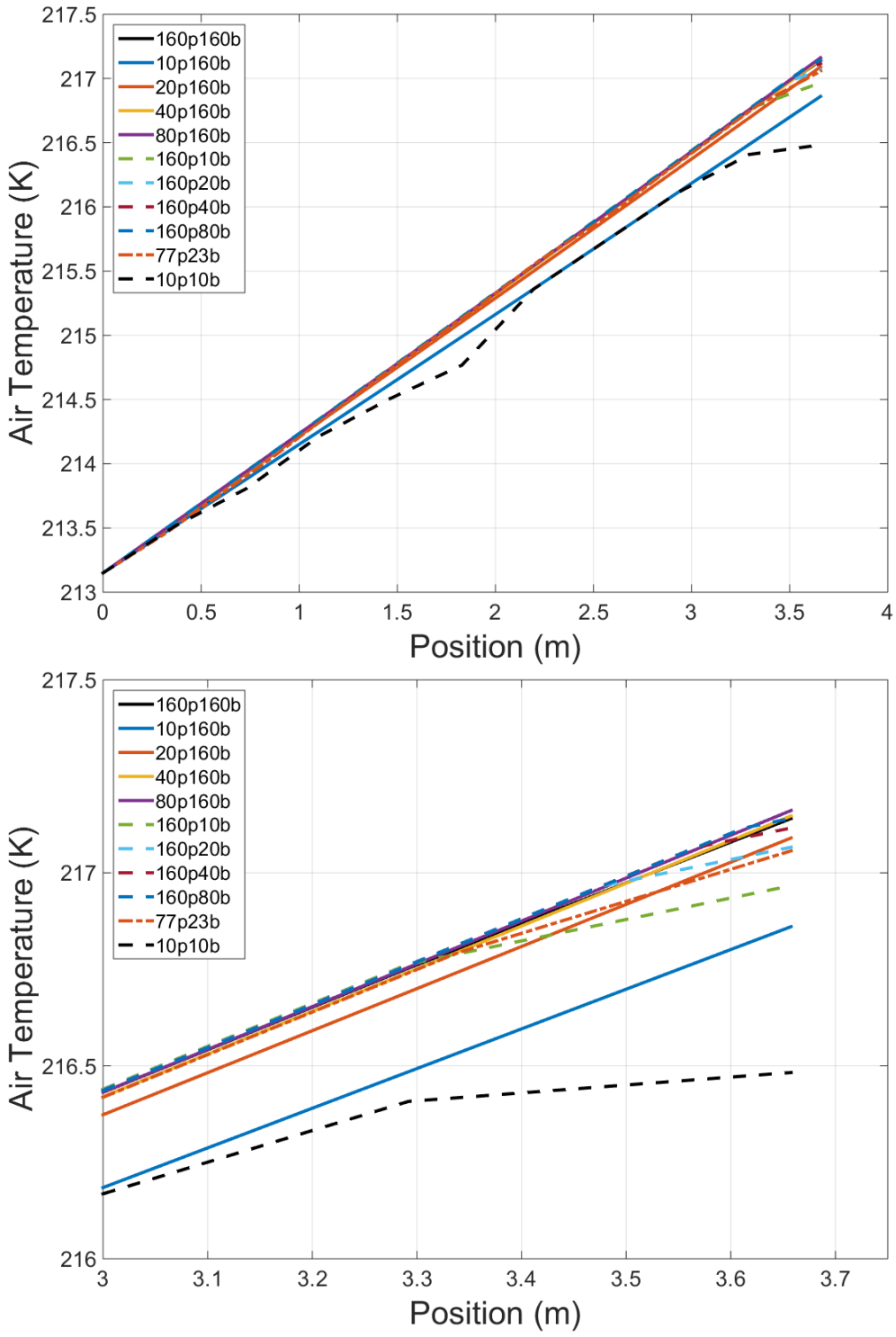

Figure 18. The air temperature profile for the entire pipe length (top) and the last 0.6576 m (bottom) at the pipe exit for all cases in Table 1.

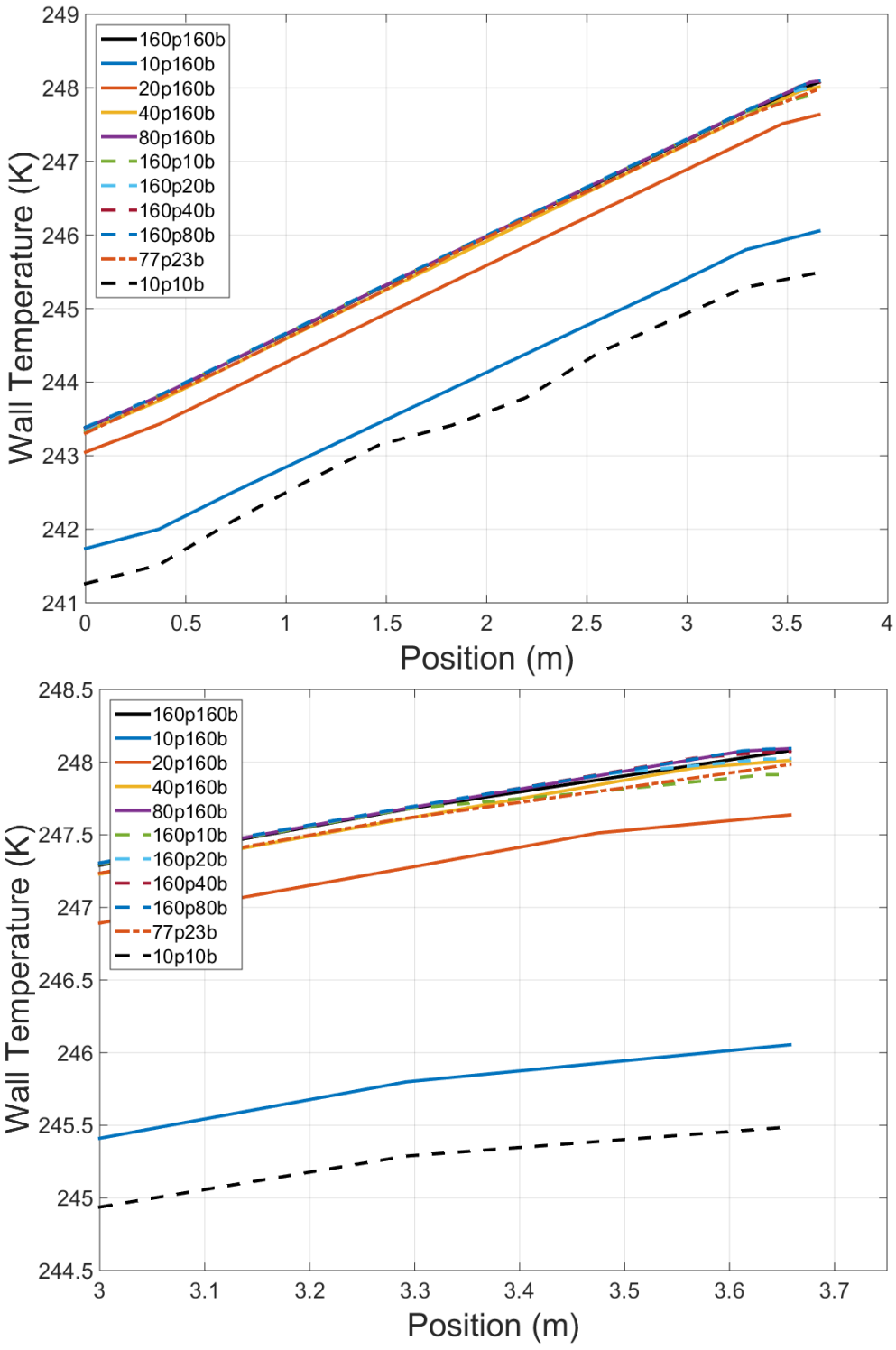

Figure 19. The wall temperature profile for the entire pipe length (top) and the last 0.6576 m (bottom) at the pipe exit for all cases in Table 1.

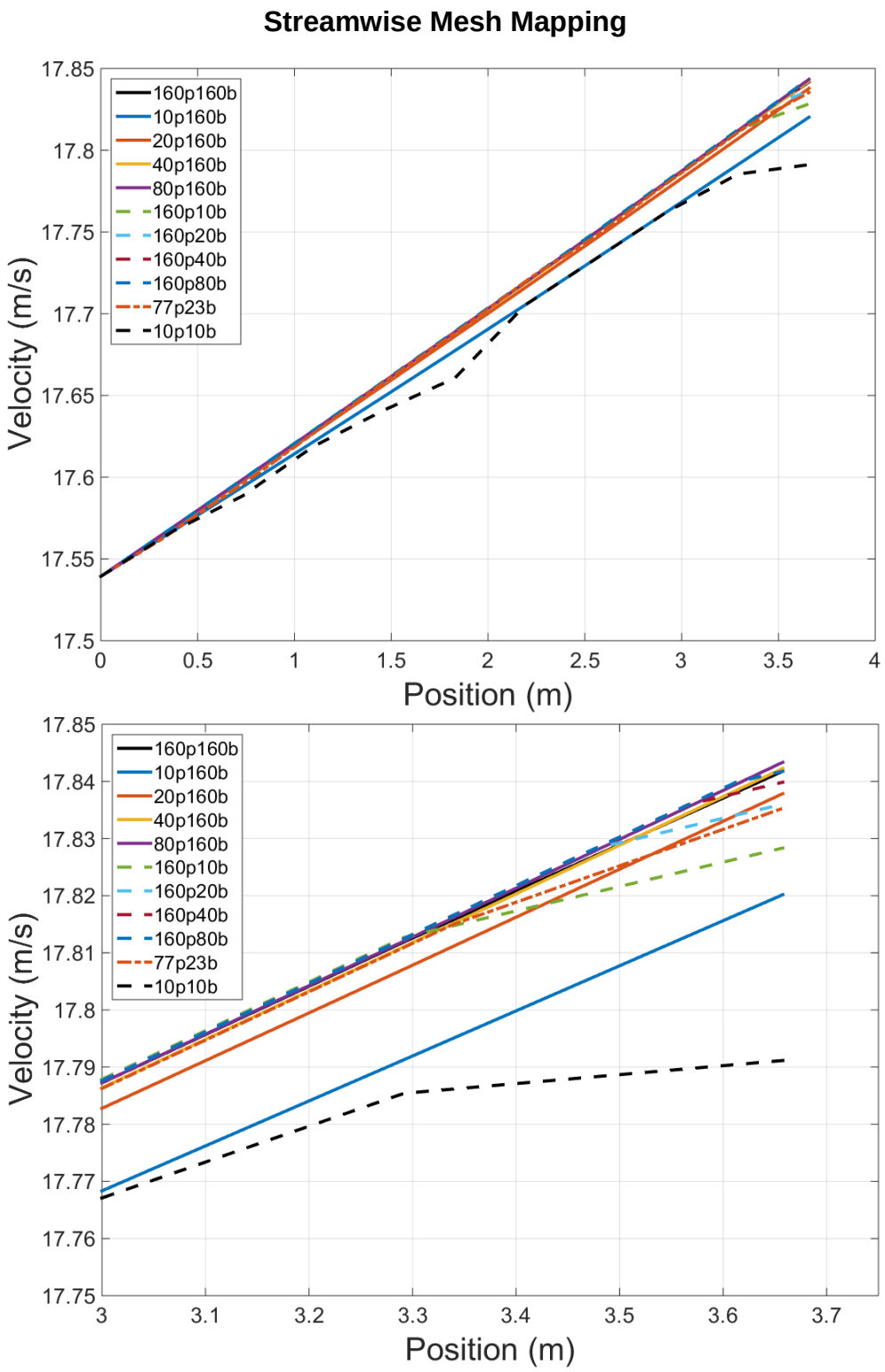

Figure 20. The velocity profile for the entire pipe length (top) and the last 0.6576 m (bottom) at the pipe exit for all cases in Table 1.

Finally, the mapping of the bar nodes to the surrounding surfaces was examined for annular flow and pipe flow using tetrahedral elements. The results are visually depicted in Figure 21. For the annular flow depicted in

Figure 21a (the outer pipe is depicted in the top of Figure 21a and the inner volume is depicted in the bottom of Figure 21a), 77 elements were used in the pipe axially, 23 bar elements were used for the fluid, and 44 elements of varying length were used in the inner volume. The inner volume also had a parabolic profile along the length of the pipe. The mapping for this case occurred as expected for both the outer pipe and the inner volume. Note that despite using the same number of elements in the pipe and fluid as the pipe flow example in Figure 14d, no defects were observed in the center of the pipe indicating that the defect did not occur consistently. In any case, analysts should avoid situations were surfaces may be equidistant between two bar nodes. For the case of pipe flow using tetrahedral elements in the pipe depicted in Figure 21b, the mapping occurred as expected. However, unlike the cases with hexahedral elements, a saw tooth mapping occurred that was more evident as the mesh became coarser.

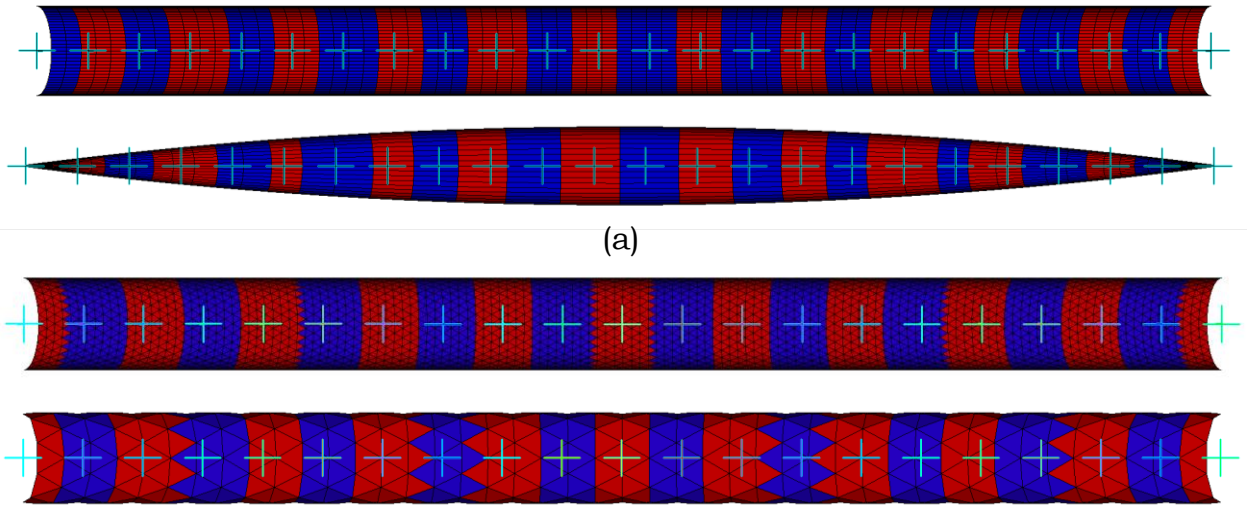

(a)

(b)

Figure 21. Graphical depictions of the mapping of bar nodes to the surrounding surfaces for (a) annular flow and (b) pipe flow using tetrahedral elements in the pipe

CFD Solution Comparison

One standard type of code verification test that is commonly used is to compare solutions between an existing (and possibly verified) software package that uses the same physical model, often described as code to code benchmarking. Dean Dobranich has explored this type of verification using SAFSIM which features a very similar physical 1D fluid flow model in Reference 1 for simple pipe flow with a similar geometry to that investigated in this document. From this work, it was shown that solutions obtained with both Aria and SAFSIM provided comparable solutions in the fluid and solid temperatures. The study described in this section is intended to test the adequacy of the advective bar elements as a low order approximation of a fully coupled 3D fluid flow simulations for relevant geometries. A series of CFD simulations using the commercial software package ANSYS Fluent® 15.0 were performed and compared against solutions from Aria using advective bar elements. While this type of comparison doesn't definitively indicate errors in the implementation of advective bars into Aria, it does provide confidence to analysts that the advective bars have been properly integrated for geometries where 3D effects of internal fluid flow should be negligible.

There are a number of significant differences between the simulations performed using Aria and Fluent. Primarily, Aria uses the finite element method and Fluent uses the finite volume method to discretize the equations for fluid flow. The equations for fluid flow evaluated in Aria are 1D in space where the equations evaluated for the fluid volume in Fluent are 3D in space. As a result, solutions from Aria are only able to provide fluid temperatures and velocities that are averaged over the cross section of the flow. To capture effects that depend on the velocity and thermal boundary layers in the fluid (like the heat transfer with the surrounding surfaces), the advective bars utilize empirical correlations for the heat transfer coefficient (HTC) for an applicable geometry. Therefore, the accuracy of the simulation is largely dependent on the availability and accuracy of the empirical HTC correlations used in the simulation.

The geometries explored here featured simple pipe flow and annular flow consistent with problems examined in previous sections of this document. Despite only modeling average temperatures and velocities in the fluid, modeling these geometries that exhibit unidirectional (*i.e.* 1D) flow with advective bar elements using appropriate empirical heat transfer coefficient correlations should produce comparable solutions to those given in Fluent.

Pipe Flow

The first geometry that was considered for this comparison was simple pipe flow. The pipe flow problem used in the mesh resolution study and depicted in Figure 1 was considered here again. To reiterate, air at an inlet temperature T_i of 213.15 K and inlet pressure p_i of 0.84 atm (85.11 kPa) flowed through a

stainless steel pipe at an initial temperature $T(r,\theta,z,0)$ of 323 K. The pipe length L was 3.6576 m and had an inner diameter D_i and outer diameter D_o of 0.28 m and 0.3 m, respectively. The pipe was assumed to be well insulated, so adiabatic boundary conditions were implemented on the outer surface of the pipe and at the inlet and outlet to the pipe. Convective heat transfer occurred on the inside surface of the pipe from the flowing air. The relevant solutions from the simulations for this problem included the outside temperature of the pipe wall, the average temperature of the air, and the average velocity of the air over the 1200 s.

Three mass flow rates $\dot{m}$ = 0.15, 1.5, and 12.5 kg/s were explored providing Reynolds numbers Re of 4.878×10^4, 4.878×10^5, and 4.065×10^6 and Mach numbers M of 0.006, 0.060 and 0.500, respectively. The purpose of investigating different Mach numbers up to 0.5 was to explore how the solution changed as the fluid velocity was approaching values where compressible effects could be significant. In addition, the problem was explored with and without a volumetric heat source q''' = 5×10^5 W/m^3 in the pipe. Therefore, in total, 6 distinct cases were compared for pipe flow. They are summarized in Table 2.

Table 2. Summary of the Pipe Flow Parameters

Case #	$\dot{m}$ (kg/s)	Re	M	q''' (W/m^3)
1	0.15	4.878×10^4	0.006	-
2	1.5	4.878×10^5	0.06	-
3	12.5	4.065×10^6	0.5	-
4	0.15	4.878×10^4	0.006	5×10^5
5	1.5	4.878×10^5	0.06	5×10^5
6	12.5	4.065×10^6	0.5	5×10^5

For the solution comparison, temperatures on the outside pipe surface were compared at 11 equally spaced locations along the length of the pipe. In addition, the average temperature and velocity from the solutions in Fluent at those same 11 axial locations were compared to the values computed in Aria. 2D axisymmetric simulations in Fluent would have been sufficient to simulate the pipe flow problem examined here (as well as the geometry for annular flow); however, using 3D simulations left open the possibility of exploring non-axisymmetric boundary conditions in future efforts using the same meshes (*e.g.* surface heat fluxes on one side of the pipe). In addition, the simple geometries explored here did not constitute a significant increase in computation time to necessitate 2D simulations.

The meshes used for these simulations are depicted in Figure 22. The advective bar mesh used a total of 51,280 elements with 160 hexahedral

elements in the pipe and 80 bar elements in the air volume along the length of the pipe. Solutions from preceding discussion on the streamwise mesh mapping showed that increasing the mesh resolution further would not yield significantly different results using advective bar elements. In the mesh for Fluent, special attention was paid to the boundary layer in the air volume. To assure the velocity profile is resolved all the way to the wall,[14] the thickness of the first cell next to the pipe wall was set to 4 μm providing non-dimensional wall distances $y^+<1$ for all mass flow rates considered here. The non-dimensional wall distance y^+ is defined as

$$y^+ = \sqrt{\frac{\tau_w}{\rho}}\frac{y}{\nu} \tag{6}$$

where τ_w is the wall shear stress, ρ is the fluid density, y is the wall normal coordinate, and ν is the kinematic viscosity. The cell thickness then expands by 20% for each successive layer to the bulk volume. The final mesh was comprised of ~3.68×10^5 cells with 88 cells along the length of the pipe.

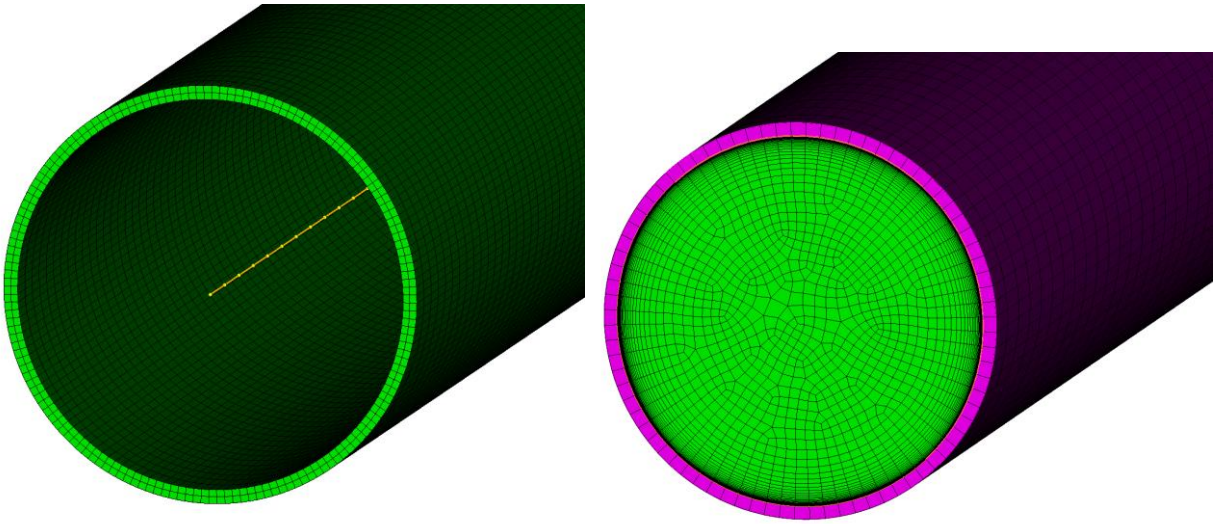

Figure 22. Mesh used in Aria with the advective bar elements (left) and the mesh used in Fluent (right)

The realizable k-ε turbulence model[15] was used for the simulations in Fluent with Fluent's proprietary 'enhanced wall treatment' option. The realizable k-ε model is a well-known Reynolds averaged Navier-Stokes turbulence model that is generally regarded as superior to other models in the k-ε family (Reference 14). According to the Fluent user manual, enhanced wall

[14] ANSYS 15.0 Release Documentation, "Fluent Theory Guide," ANSYS Inc.

[15] Shih, T., et al., "A New k-ε Eddy Viscosity Model for High Reynolds Number Turbulent Flows", Computers Fluids, 24(3), 227-238, (1995)

treatment resolves the velocity profile of the fluid all the way to the wall if the mesh is sufficiently fine ($y^+<1$), and used semi-empirical wall functions in areas where the mesh is not sufficiently fine. This allows more flexibility when meshing complex geometries. However, since a cell thickness at the wall was set such that $y^+<1$ in all areas of the geometry, wall functions were not needed for this model.

For each respective mass flow rate, a steady-state simulation was first performed for a pipe without any heat transfer occurring. The pipe used in these steady-state simulations possessed the same diameter as previously discussed and a length of 25 m. The fully-developed velocity profile at the outlet of the pipe from these simulations was then used as the inlet boundary condition for the transient simulations. For the advective bar simulations, the Gnielinski correlation for pipe flow (Reference 13) was used as implemented in Aria.[16]

To assure a sufficiently fine mesh was created for the simulations in Fluent, several preliminary steady-state simulations were performed with a mass flow rate of 1.5 kg/s and without a volumetric heat source in the pipe volume for a series of refined meshes. The pipe temperature was set equal to the fluid, so heat transfer did not occur. For the set of refined meshes, the cell size growth rate was increased from the defined first wall cell thickness of 4 μm to determine if the velocity profile would change near the wall. The growth rates investigated included 10%, 15%, 20%, 25%, 40%, and 60%. The resulting velocity profile near the wall from r = 0.138 to 0.139 was then plotted in Figure 23. As observed in the figure, there was very little change in the velocity profile for the range of growth rates explored and the velocity profile appeared to be converging as the growth rate decreased. From this figure, a growth rate of 20% was chosen.

[16] Notz, P., et al., "SIERRA Multimechanics Module: Aria User Manual – Version 4.36", SAND2007-xxxx, Printed April 2015

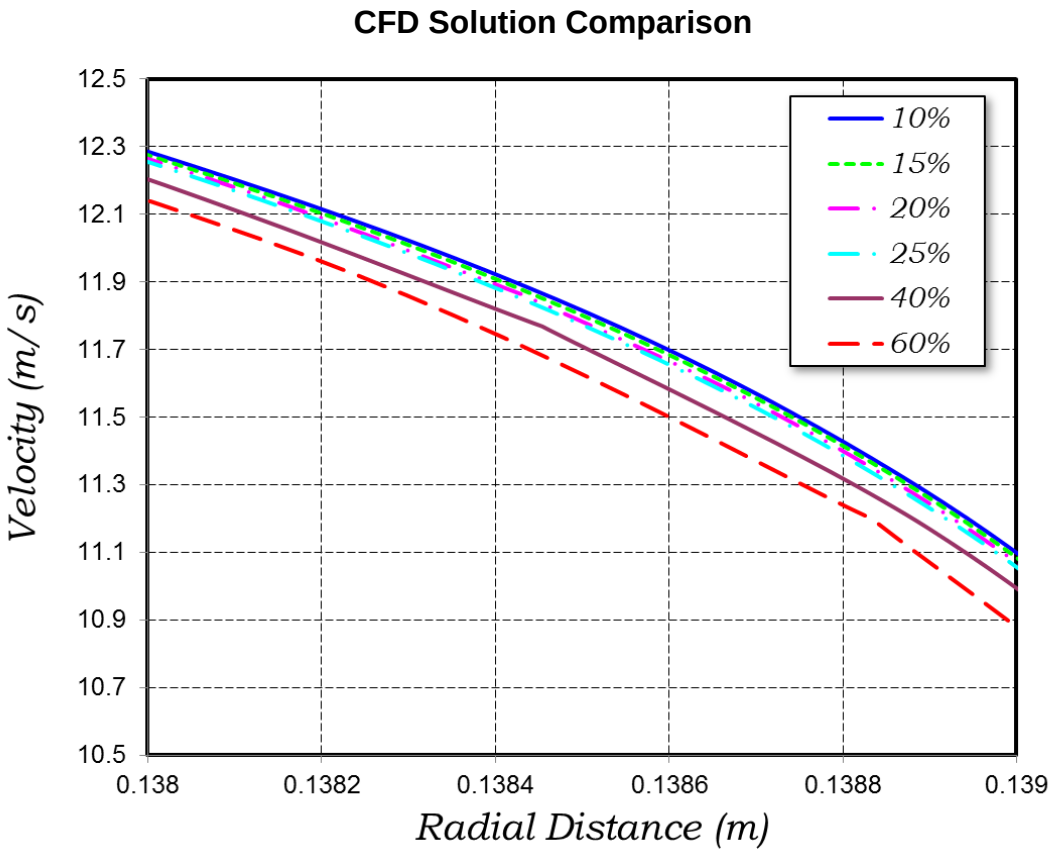

Figure 23. Velocity profile near the wall for different mesh growth rates

In addition to the growth rate of the cells from the pipe wall, the number of cells along the length of the pipe was investigated. Another series of simulations was performed using a set of refined meshes. In these transient simulations, heat transfer was allowed between the hot pipe at 323 K and the fluid entering at 213.15 K. The number of cells investigated ranged from 11 to 176 in the streamwise direction and varied uniformly. The outside temperature profile of the pipe wall at the start of the pipe ($z = 0$ m), at the middle of the pipe ($z = 1.8288$ m), and at the exit of the pipe ($z = 3.6576$ m) is plotted in Figure 24. Very little change in the temperature profile was observed at the middle of the pipe and at the exit of the pipe. However, at the start of the pipe, where the thermal boundary layer was beginning to form, the number of cells axially along the pipe has a large effect on the temperature profile. Based on Figure 24, it was observed that the temperature profile appeared to be converging as the number of cells increased and 88 cells was deemed sufficient to compare with Aria.

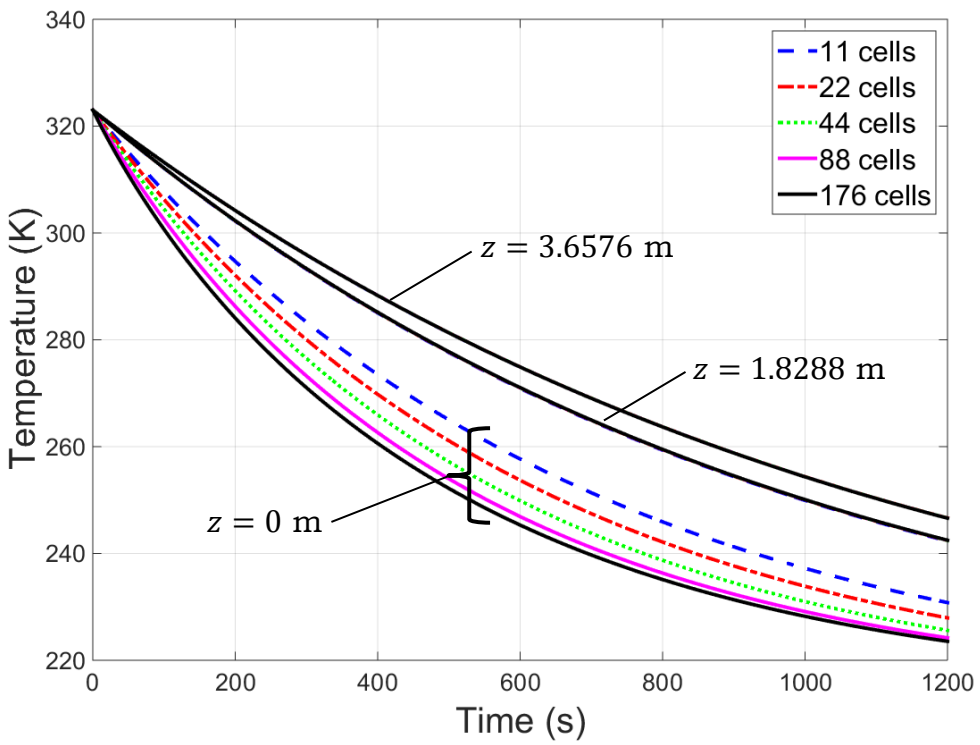

Figure 24. Temperature profile of the pipe at z = 0 m, z = 1.8288 m, and z = 3.6576 m for different number of cells in the streamwise direction

Using the preceding mesh parameters with Fluent, simulations were performed for $\dot{m}$ = 0.15, 1.5, and 12.5 kg/s and compared to solutions using advective bars in Aria. First, the cases without a volumetric heat source in the pipe were examined. The temperature profile on the exterior of the pipe, the average air temperature, and the average velocity profile were compared at z = 0, $L/2$, and L. The results for $\dot{m}$ = 1.5 kg/s are presented in Figure 25-27. The results for $\dot{m}$ = 12.5 kg/s are presented in Figure 28-30. The results for $\dot{m}$ = 0.15 kg/s are presented in Figure 31-33. Recall that since the two software packages used different physical models, the solutions for the following figures were expected to have some deviation in the temperature and velocity profiles; however, the fundamental behavior of the solutions should be similar.

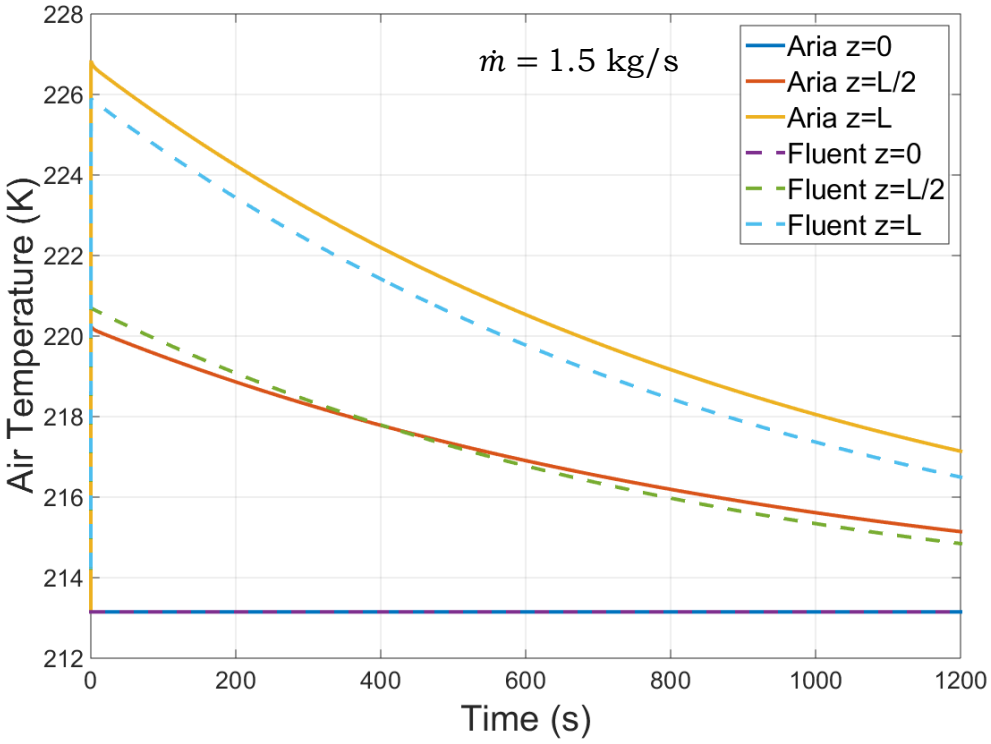

Figure 25. Air temperature profiles with time for ṁ = 1.5 kg/s at different axial locations

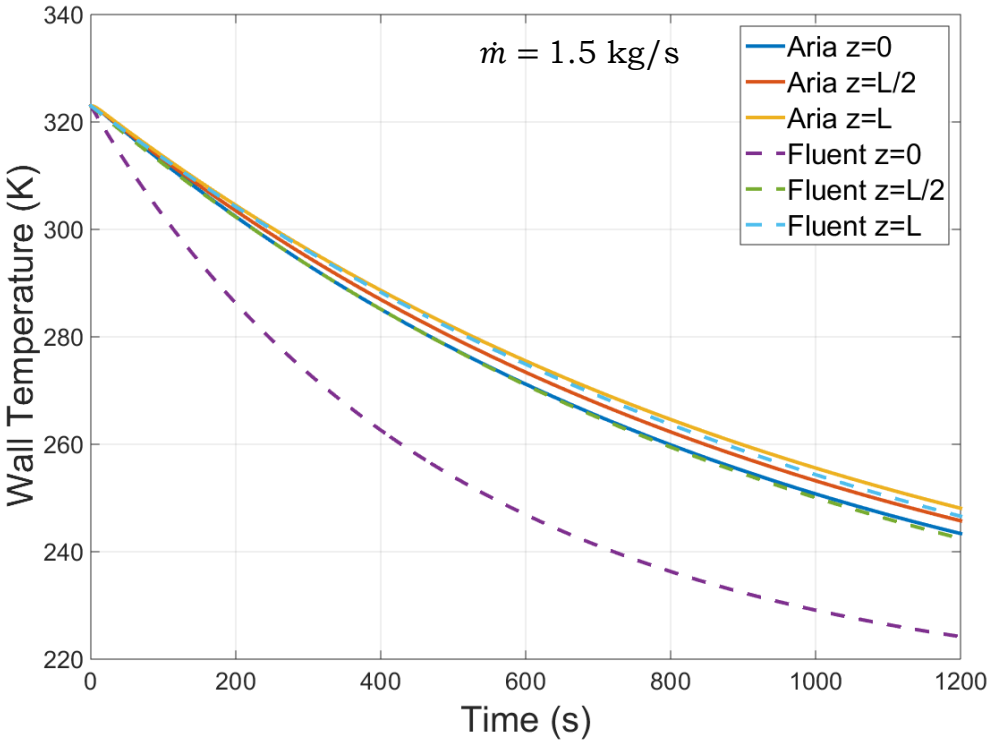

Figure 26. Exterior pipe temperature profiles with time for ṁ = 1.5 kg/s at different axial locations

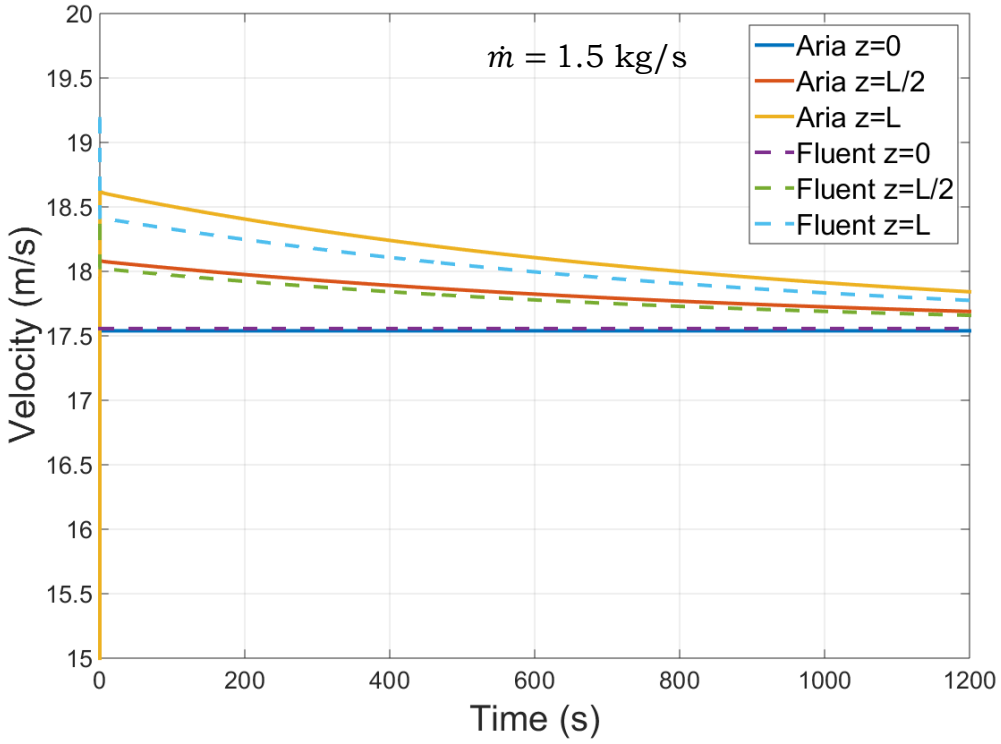

Figure 27. Velocity profiles with time for ṁ = 1.5 kg/s at different axial locations

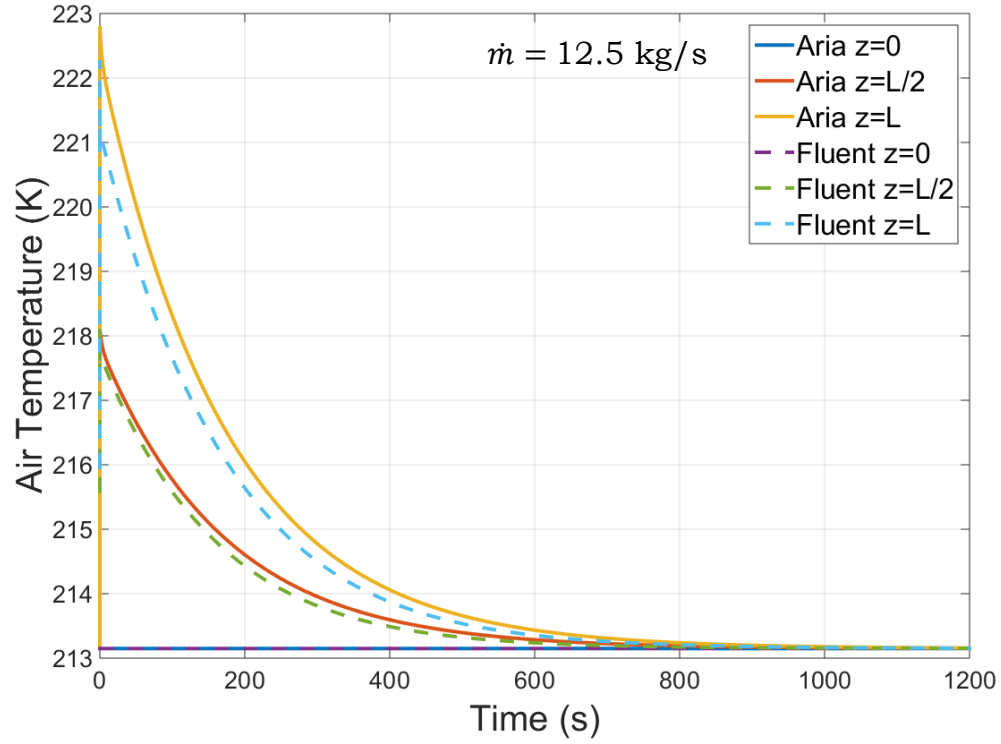

Figure 28. Air temperature profiles with time for ṁ = 12.5 kg/s at different axial locations

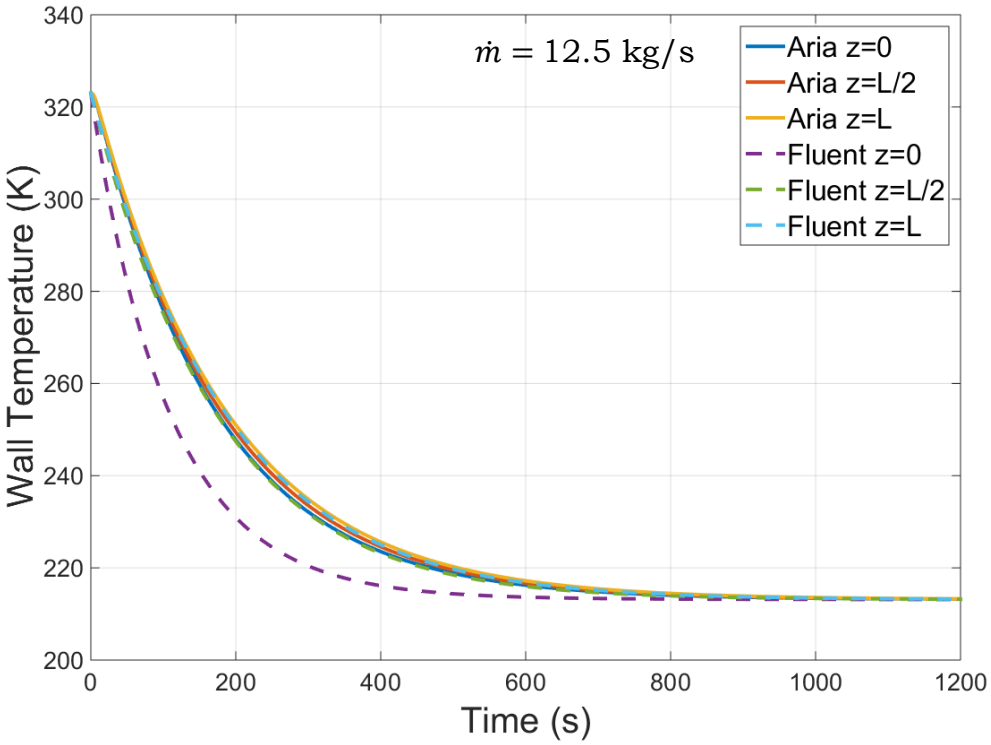

Figure 29. Exterior pipe temperature profiles with time for ṁ = 12.5 kg/s at different axial locations

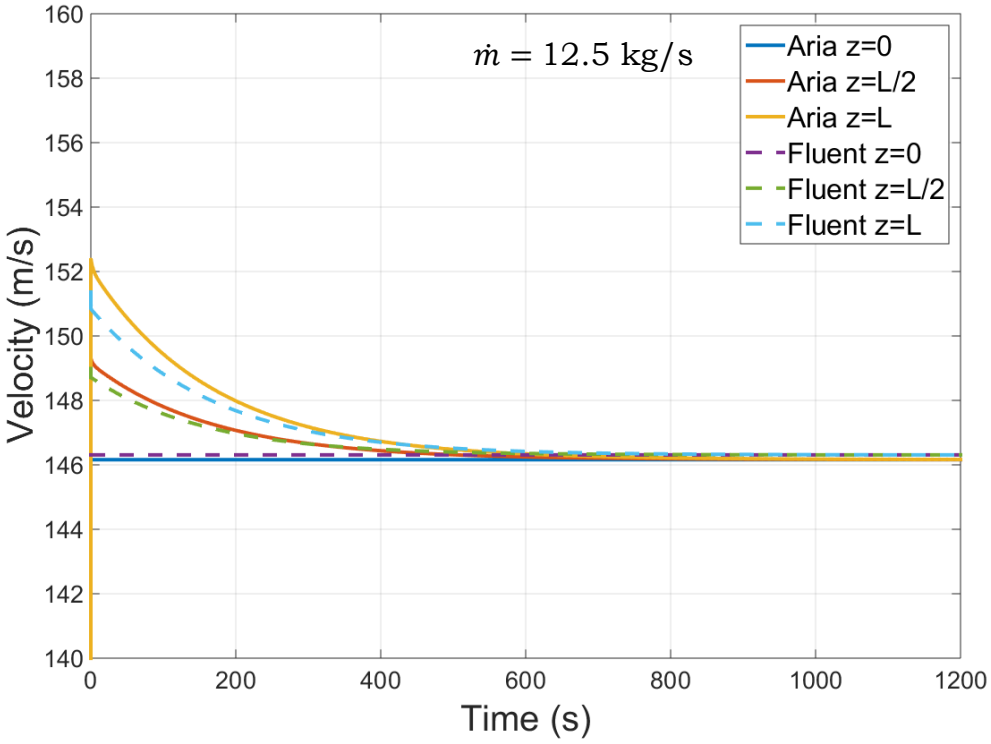

Figure 30. Velocity profiles with time for ṁ = 12.5 kg/s at different axial locations

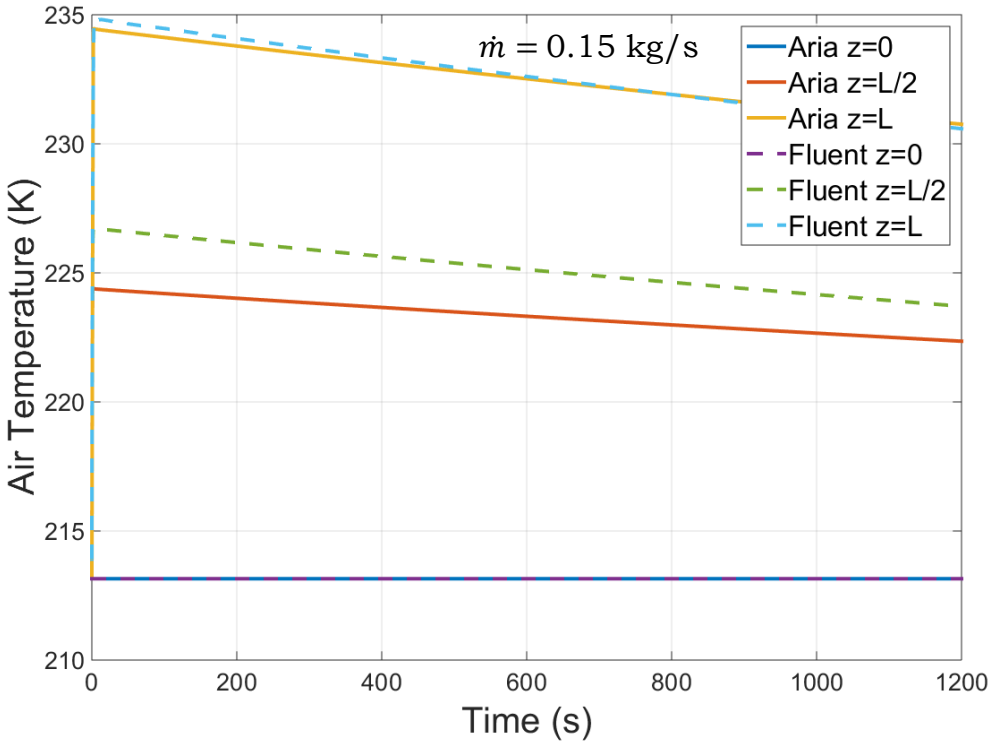

Figure 31. Air temperature profiles with time for ṁ = 0.15 kg/s at different axial locations

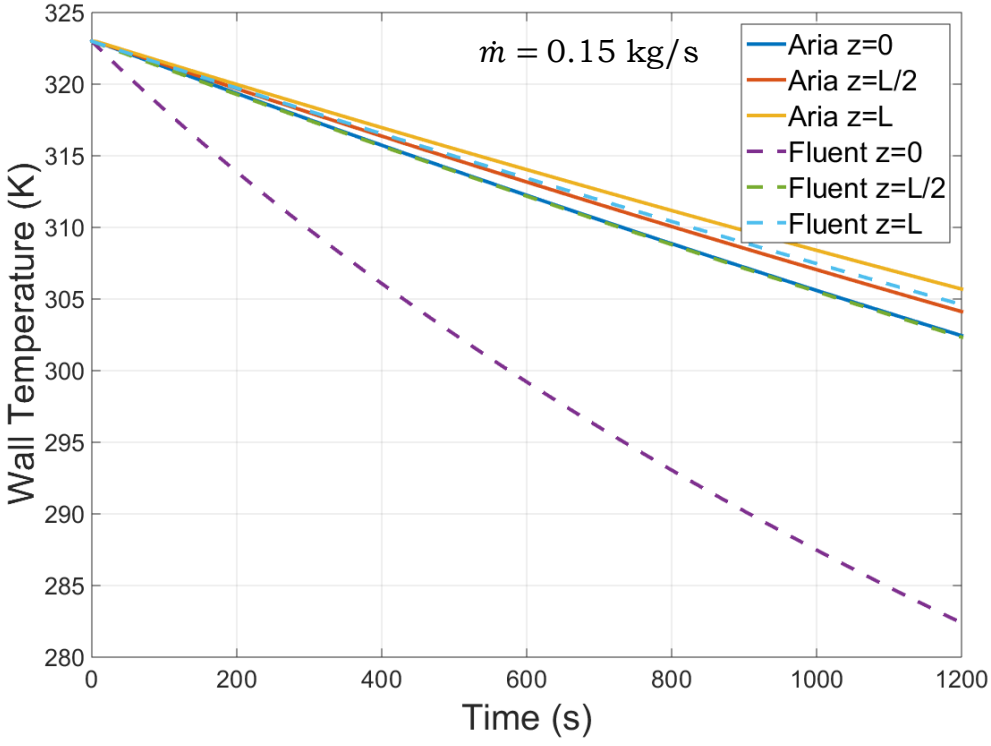

Figure 32. Exterior pipe temperature profiles with time for ṁ = 0.15 kg/s at different axial locations

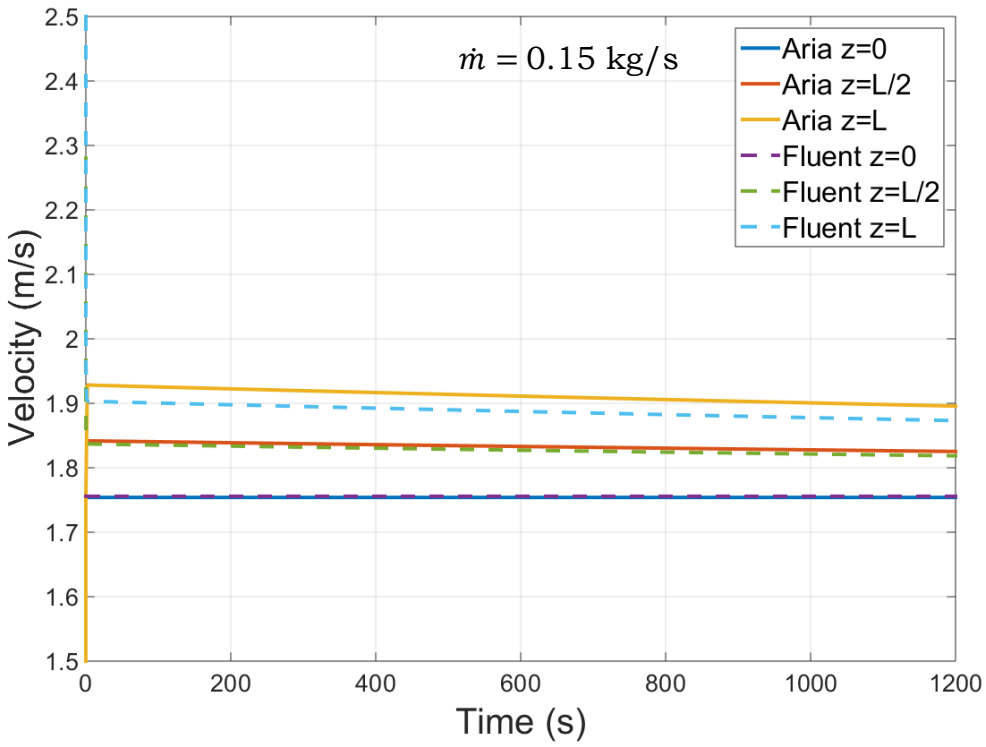

Figure 33. Velocity profiles with time for ṁ = 0.15 kg/s at different axial locations

From the previous nine figures, the solutions from Aria for the air temperature were observed to be similar to the solutions produced in Fluent. Deviation up to 3°C was observed at lower flow rates near the start of the pipe, but the air temperature profiles agreed well. The wall temperature in the pipe showed good agreement for all three flow rates with the exception of $z = 0$. This discrepancy at the start of the pipe was largely explained by the heat transfer coefficient correlation used in simulation. The Gnielinski correlation provided in Aria was developed for thermally fully developed flow. However, at the start of the pipe where thermal entrance effects were expected, the local heat transfer coefficient will differ from the fully thermally developed value for pipe flow. As the flow develops along the length of the pipe the local HTC should approach the fully developed value. Table 3 presents the local HTC along the length of the pipe as calculated by Fluent and the Gnielinski correlation provided in Aria for $\dot{m} = 1.5$ kg/s. As the flow moved axially along the length of the pipe in Fluent, the local HTC decreased rapidly and asymptotically approached a value close to that predicted by the Gnielinski correlation. This behavior was consistent with that for thermally developing pipe flow.[17] In addition, it was observed that in all the previous figures of the wall temperature, the temperatures predicted with Aria were higher than that of

[17] Incropera, F., et al., Fundamentals of Heat and Mass Transfer, John Wiley & Sons, Inc., 6th Edition, Hoboken, New Jersey, 2007.

Fluent. Arguably, with a more accurate HTC correlation that accounts for thermally developing flow the temperature profile of the wall would be more accurate. An entrance correction factor f_E has recently been integrated into Aria that may be used to approximately account for thermally developing flows defined by

$$f_E = 1 + \left(\frac{D_h}{L_E} \right)^{2/3} \tag{7}$$

where D_h is the hydraulic diameter and L_E is the distance from the entrance. However, as this correction factor was relatively new at the time of writing this document, it was not applied in the simulations performed here.

Table 3. Local Heat Transfer Coefficient along the Pipe Length at t =1200 s

Heat Transfer Coefficient (W/m²K), $\dot{m}$ = 1.5 kg/s			
z	Fluent	Gnielinski	Gnielinski w/ f_E
0	85.50	44.66	89.32
L/10	59.44	44.68	82.07
L/2	49.96	44.74	57.54
L	46.89	44.82	52.90

The last column in Table 3 multiplied the values calculated with the Gnielinski correlation by f_E to approximate values of the HTC including thermally developing flow. Note that at the start of the pipe (z = 0), f_E will approach infinity and must be capped to a constant. For the values provided in Table 3, f_E was capped to a multiple of two. Although the values for the HTC including thermally developing flow were higher than those predicted by Fluent, particularly for z = L/10, it provided an improved estimate for thermally developing flow. Including further correction factors to account for changes in properties that occur over the thermal boundary layer (a 'film coefficient') for cooling gasses, which were applicable to this problem, would improve agreement between Fluent and the correlation. This is discussed in more detail later in the document.

To confirm that thermally developing flow resulted in the differences in temperature at the start of the pipe, the HTC calculated from the simulations in Fluent was used in lieu of the Gnielinski correlation in the advective bar model for $\dot{m}$ = 1.5 kg/s. The inner surface of the pipe was divided into 11 sections axially and the corresponding average HTC values from Fluent were used for each respective section. The pipe temperature is again plotted in Figure 34 including the solution from Aria using HTCs calculated in Fluent. As observed in Figure 34, the solution near the entrance to the pipe (z = 0 m) is

significantly closer to the solution from Fluent deviating by ~2°C. This emphasized both the importance of an accurate empirical HTC correlation and the capability of the advective bar elements in modeling pipe flow with an appropriate correlation. This result also stressed the need for the new correction factors that account for thermally developing flow to use with the advective bar element model.

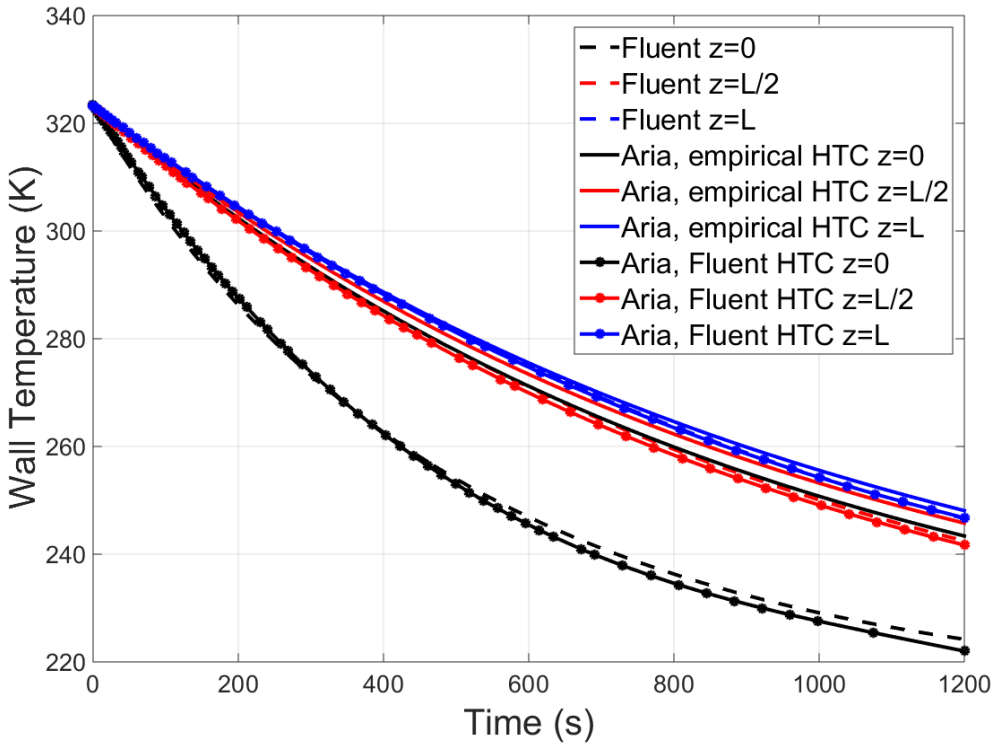

Figure 34. Exterior pipe temperature profiles with time for ṁ = 1.5 kg/s at different axial locations. Solution with advective bars in Aria is given using an empirical HTC correlation (solid lines) and HTCs from Fluent (lines with markers)

Finally, the average velocity profiles from Aria, which did not vary significantly along the length of the pipe, agreed closely with the Fluent results for all three flow rates. The largest deviations were observed near the exit of the pipe. For $\dot{m}$ = 12.5 kg/s (M = 0.5), any significant effects from compressibility were not observed.

The temperature profiles for pipe flow were also compared with the addition of a volumetric heat source of 5×10^5 W/m^3 in the pipe. For brevity and given the relative agreement for all three flow rates without a volumetric source, only the results for $\dot{m}$ = 1.5 kg/s are provided in following three figures. However, a similar behavior in the temperature and velocity profiles was observed in all three mass flow rates.

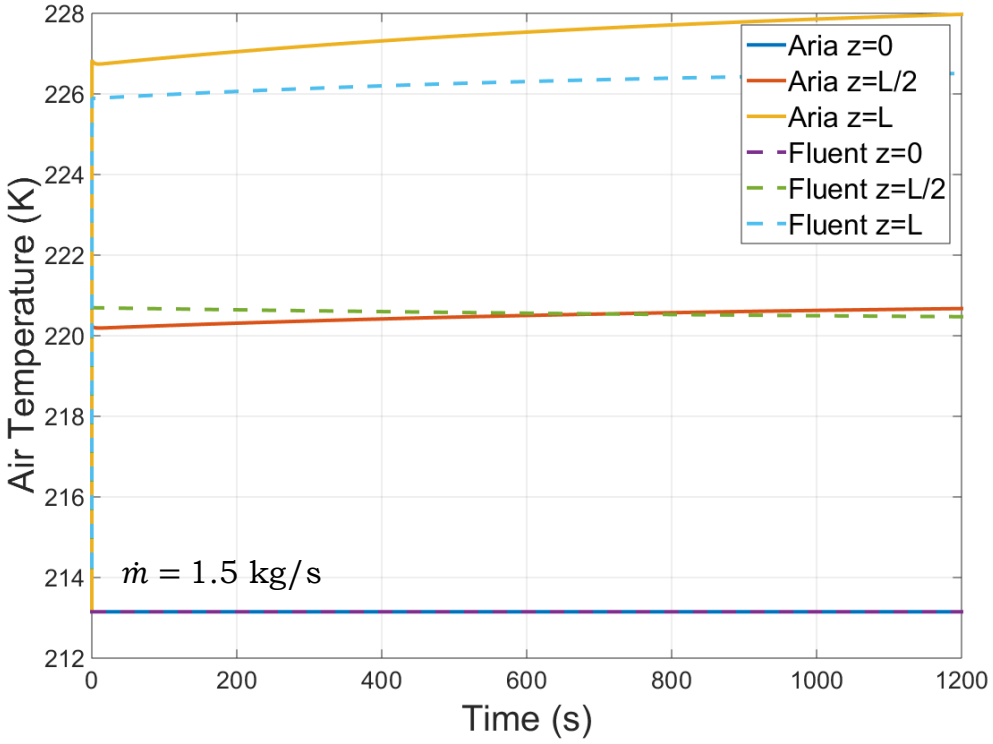

Figure 35. Air temperature profiles with time for ṁ = 1.5 kg/s at different axial locations with a 5×10^5 W/m^3 volumetric heat source

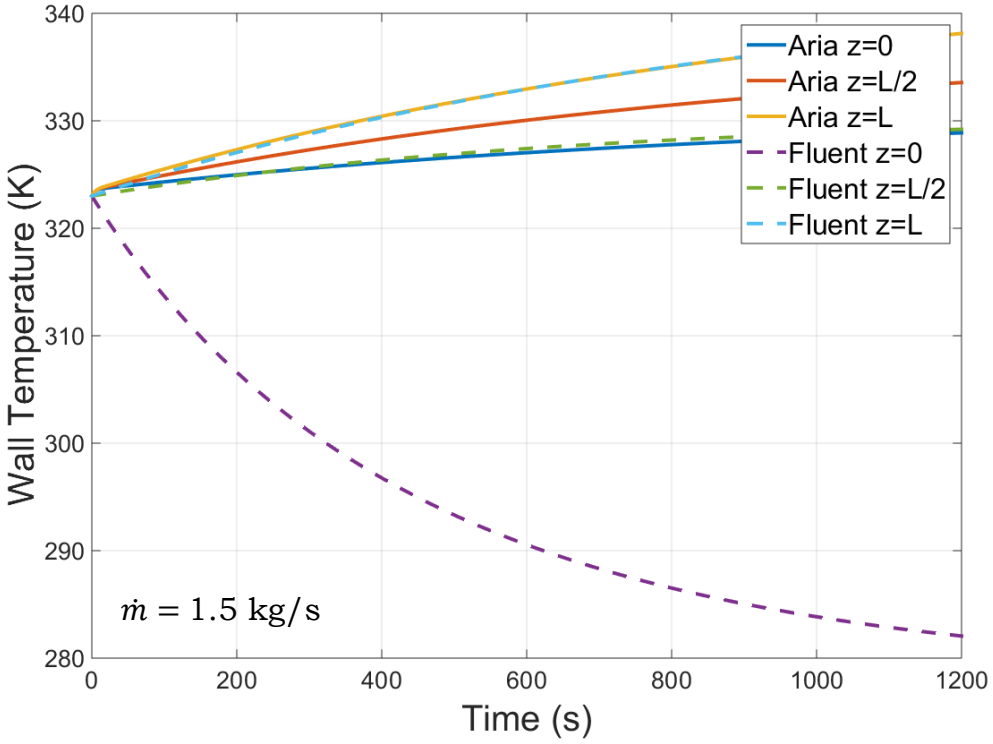

Figure 36. Exterior pipe temperature profiles with time for ṁ = 1.5 kg/s at different axial locations with a 5×10^5 W/m^3 volumetric heat source

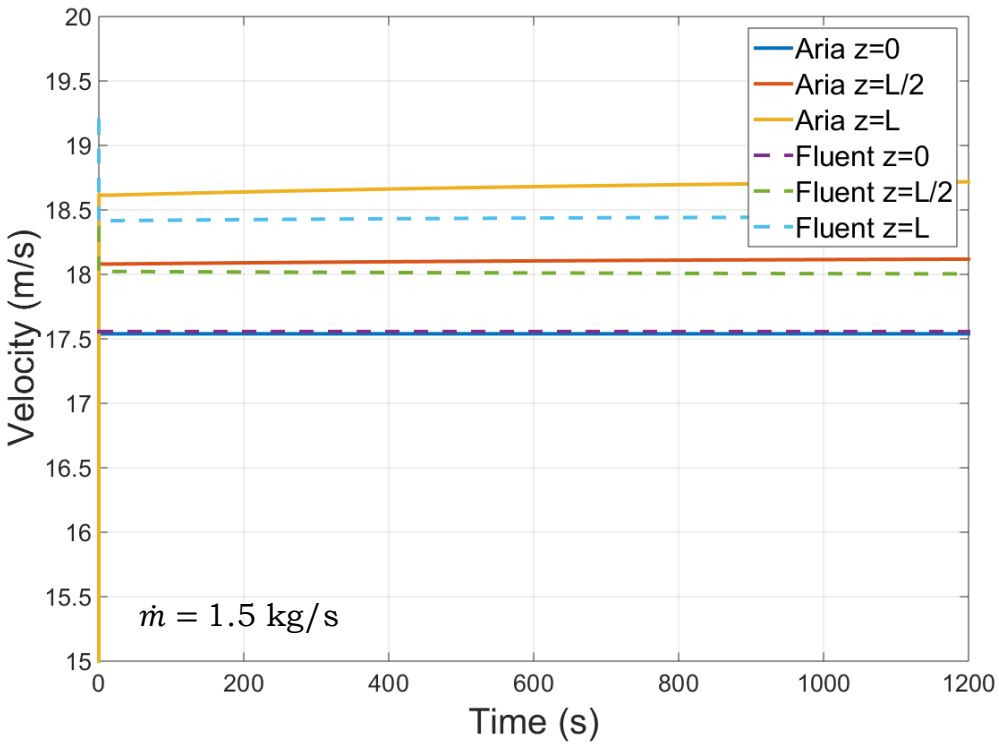

Figure 37. Velocity profiles with time for ṁ = 1.5 kg/s at different axial locations with a 5×10^5 W/m^3 volumetric heat source

Including a volumetric heat source, the solutions from the advective bar elements in Aria again showed good agreement with the solutions from Fluent with the exception of the wall temperature near the start of the pipe. Again, this was explained by the lack of a HTC correlation in Aria capable of predicting thermally developing flow (see Figure 34). Near the exit of the pipe, the temperature profiles were very similar. One might question why the temperature profile near the end of the pipe was not significantly affected by the poor agreement at the start of the pipe. This was largely a result of the materials and geometry chosen for this problem. In particular, the very low thermal conductivity and thin wall of the pipe prevented significant axial conduction down the length of the pipe relative to the radial conduction and convection in the pipe. A lumped capacitance analysis of this pipe flow problem (performed here by Sam Subia[18]) showed that conduction axially was not significant.

Annular Flow

This study also investigated flow through an annulus. Straight annular flow was considered with dimensions in the outer pipe the same as those used

[18] Subia, S., "#13139 Unrealistic results with Advective Bar Elements", Sandia National Laboratories Internal Document, Response for Sierra Trac Ticket #12129, April 7, 2015

in the previous pipe flow problem. The annulus length L was 3.6576 m and the outer pipe had an inner diameter D_i and outer diameter D_o of 0.28 m and 0.3 m, respectively. The inner cylinder had a diameter d_o of 0.24 m. Air entered at an inlet temperature T_i of 213.15 K and inlet pressure p_i of 0.84 atm (85.11 kPa) and flowed through the stainless steel annulus at an initial temperature $T(r,\theta,z,0)$ of 323 K. Adiabatic boundary conditions were set on all the exterior surfaces of the geometry. Convection heat transfer occurred on the inside surface of the outer pipe and the outside surface of the inner cylinder.

Three mass flow rates $\dot{m}$ = 0.065, 0.65, and 3.315 kg/s were explored providing Reynolds numbers Re of 1.138×10^4, 1.138×10^5, and 5.805×10^5 and Mach numbers M of 0.01, 0.10 and 0.50, respectively. This problem was also explored using a volumetric heat source of 5×10^5 W/m^3 on all volumes in the annulus. As in the pipe flow problem, 6 distinct cases were compared for annular flow. They are summarized in Table 4.

Table 4. Summary of the Annular Flow Parameters

Case #	$\dot{m}$ (kg/s)	*Re*	*M*	q''' (W/m^3)
1	0.065	1.138×10^4	0.01	-
2	0.65	1.138×10^5	0.1	-
3	3.315	5.805×10^5	0.5	-
4	0.065	1.138×10^4	0.01	5×10^5
5	0.65	1.138×10^5	0.1	5×10^5
6	3.315	5.805×10^5	0.5	5×10^5

Temperatures and velocities were compared at the same locations as the pipe flow problem; that is, on the outside pipe at 11 equally spaced locations along the length of the pipe. In addition, the average temperature and velocity from the solutions in Fluent at those same 11 axial locations were compared to the values computed in Aria. Finally, 11 equally spaced locations were also compared at r = 0.10575 m along the length of the inner cylinder.

The meshes used for the comparison are pictured in Figure 38. For the advective bar mesh, a total of 490,720 elements with 160 hexahedral elements in the solid volumes and 80 bar elements in the air volume along the length of the pipe were used. Lessons learned from the previous mesh analysis on the pipe flow were applied to the meshes used for annular flow here in Fluent. The thickness of the first cell next to both walls was set to 4 μm providing $y^+<1$ for all mass flow rates considered here to assure the velocity profile is resolved all the way to the wall. The cell thickness then expands by 20% for each successive layer until the two layers meet. The final mesh was comprised of ~5.59×10^5 cells with 88 cells along the length of the annulus.

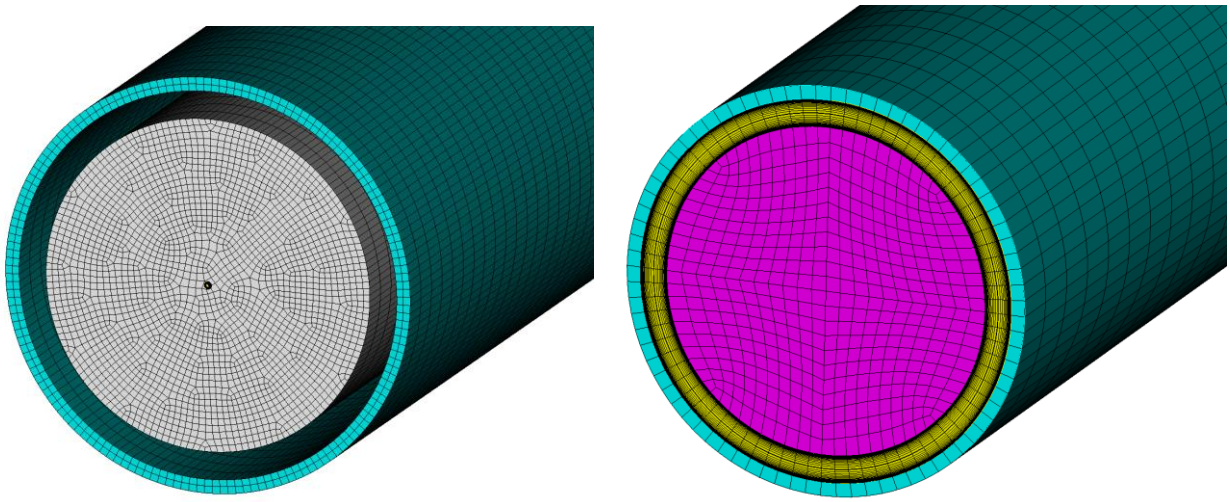

Figure 38. Meshes used in Aria with the advective bars (left) and the mesh used in Fluent (right). Bar elements are obscured by the inner cylinder

As with pipe flow, the realizable k-ε turbulence model was used for the simulations in Fluent with Fluent's proprietary enhanced wall treatment option. A cell thickness at the wall was again set such that $y^+<1$ in all areas of the geometry and wall functions were not utilized with the wall treatment option. For each respective mass flow rate, a steady-state simulation was first performed on an annulus without any heat transfer occurring. The annulus used in these steady-state simulations possessed the same diameters as previously discussed but a length of 25 m. The fully-developed velocity profile at the outlet of the annulus from these simulations was then used as the inlet boundary condition for the transient simulations. For the advective bar simulations the Gnielinski correlation for annular flow[19] was used (Reference 16).

Using the meshes depicted in Figure 38, a series of simulations were performed with Fluent for $\dot{m}$ = 0.065, 0.65, and 3.315 kg/s and compared to solutions using advective bars in Aria. First, the cases without a volumetric source were examined. For brevity, only the solutions for $\dot{m}$ = 0.65 kg/s were provided as other flow rates did not reveal any additional information (*e.g.* effects from compressibility). The temperature profile on the exterior of the pipe, the temperature in the inner cylinder, the average air temperature, and the average air velocity profile were compared. The results for $\dot{m}$ = 0.65 kg/s are presented in Figure 39-42. Recall that the two software packages use different physical models, so the solutions for the following figures were expected to have some deviation in the temperature and velocity profiles; however, the fundamental behavior of the solutions should be similar.

[19] Gnielinski, V., "Heat Transfer Coefficients for Turbulent Flow in Concentric Annular Ducts," Heat Transfer Engineering, Vol. 30, No. 6, 431-436 (2009).

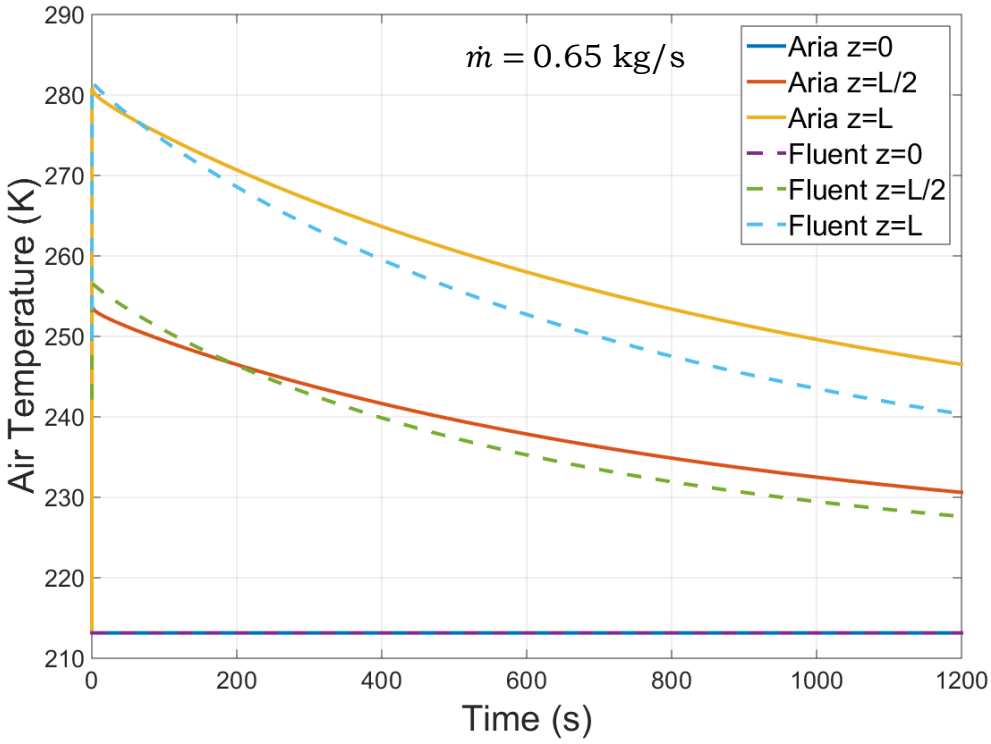

Figure 39. Air temperature profiles with time for ṁ = 0.65 kg/s at different axial locations

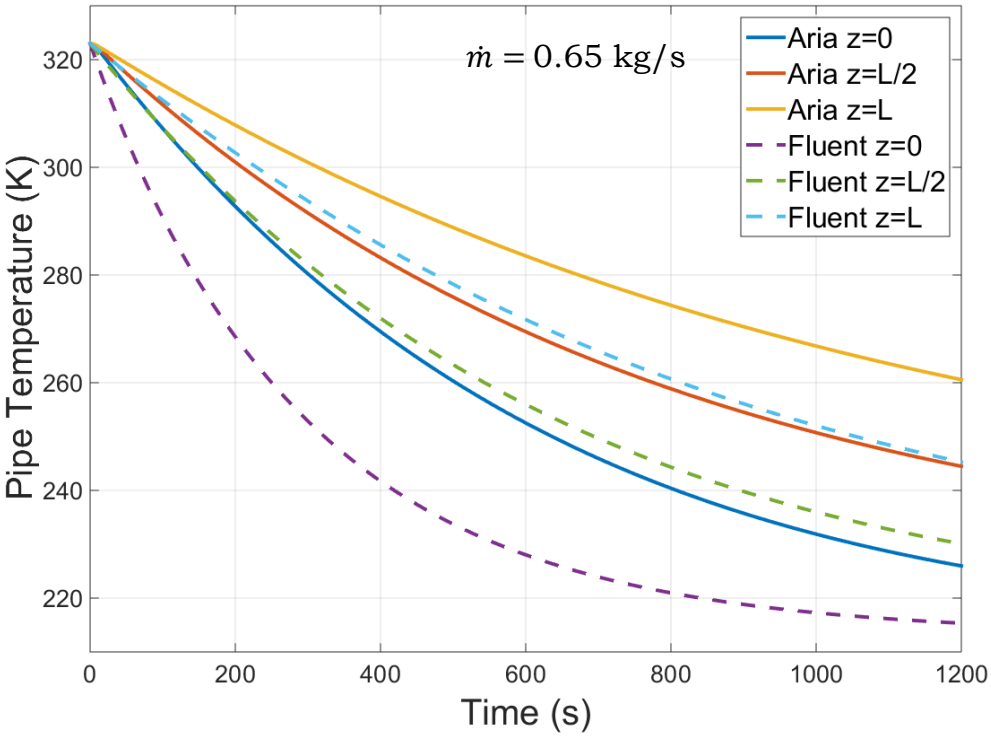

Figure 40. Pipe temperature profiles with time for ṁ = 0.65 kg/s at different axial locations

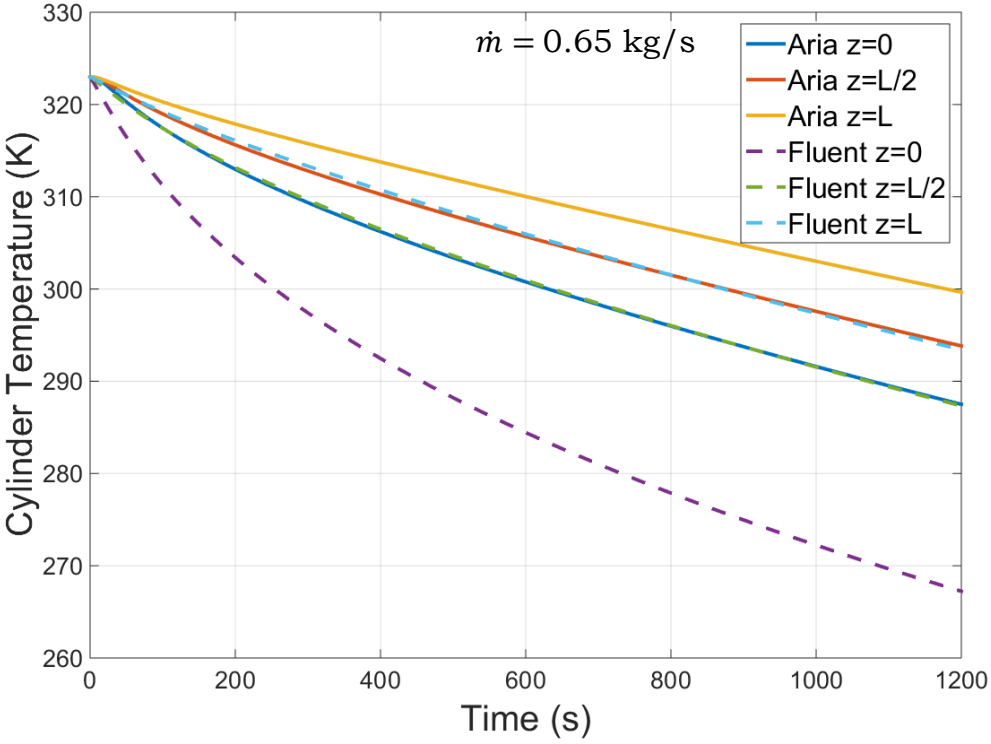

Figure 41. Inner cylinder temperature profiles with time for ṁ = 0.65 kg/s at different axial locations

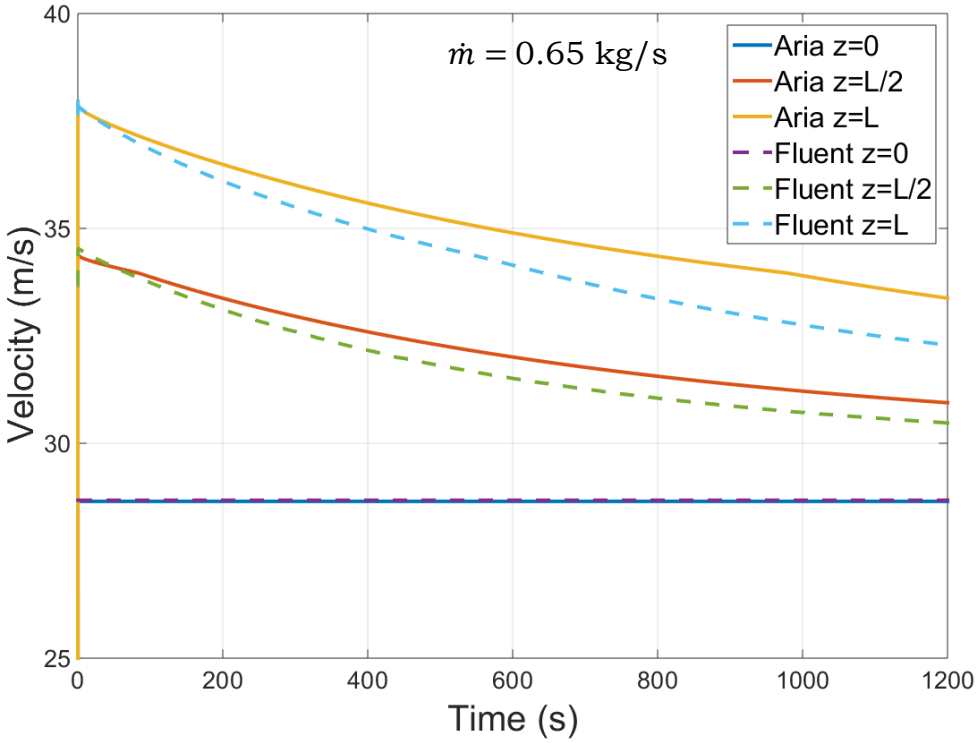

Figure 42 Velocity profiles with time for ṁ = 0.65 kg/s at different axial locations

From the previous four figures, the solutions from Aria for annular flow showed similar behavior to the solutions produced in Fluent for all temperatures and velocities; however, the difference between the solutions, particularly in the solid temperatures, was larger than that observed for pipe flow previously. Much of this difference can be attributed to the empirical HTC correlations used in the advective bar model. The HTCs for annular flow depend not only on *Re*, *Pr*, and the geometry, but also on whether heat transfer is occurring on the inner cylinder or the outer pipe. For the case when heat transfer is occurring on both surfaces, as is here, a correlation is not provided (the case for heat transfer occurring on the inner cylinder only was used here as an approximation). Furthermore, at the time of these simulations were performed, the Gnielinski correlation for annular flow also implemented a correction factor K to account for changes in properties that occur over the thermal boundary layer (a 'film coefficient') for cooling gasses defined as follows

$$K = \left(\frac{T_a}{T_w} \right)^{0.45} \quad \text{for } T_a < T_w; \; K = 1 \text{ otherwise} \tag{8}$$

where T_a is the mean air temperature and T_w is the wall temperature. The effect of this coefficient was that it tended to lower the HTC as calculated by the correlation. A lower HTC coefficient resulted in higher temperatures calculated in the solid volumes as observed in Figure 40 and Figure 41. By also including entrance effects (*e.g.* through the inclusion of the entrance effect correction factor in Eq. 7), which would increase the HTC, then the agreement between Fluent and Aria would be improved.

To illustrate this effect, the correction factors K and f_E in Eqs. 7 and 8, respectively, are plotted in Figure 43 for D_h = 0.04 m, T_w = 300 K, and T_a = 260 K. These were representative values from the annular problem investigated here. When only including K, the calculated HTC from the correlation was lower than the original value (*i.e.* the correction factor was less than 1). However, when including both K and f_E, the product of the two correction factors was higher over the length of the annulus and for the entrance it was significantly higher. Therefore, by including both correction factors in the Aria simulations, the agreement between Fluent and Aria in the solid temperatures would be improved. Notice that by not including either of these correction factors, such as in the Gnielinski correlation for pipe flow at the time of this study, then the original value of the HTC in the middle of the pipe and the exit of the pipe was approximately the same (coincidently, the product of the correction factors was approximately 1 over the length of the problem). This explained why there was still good agreement between Aria and Fluent for the pipe flow problem in the previous section at the middle and exit of the pipe.

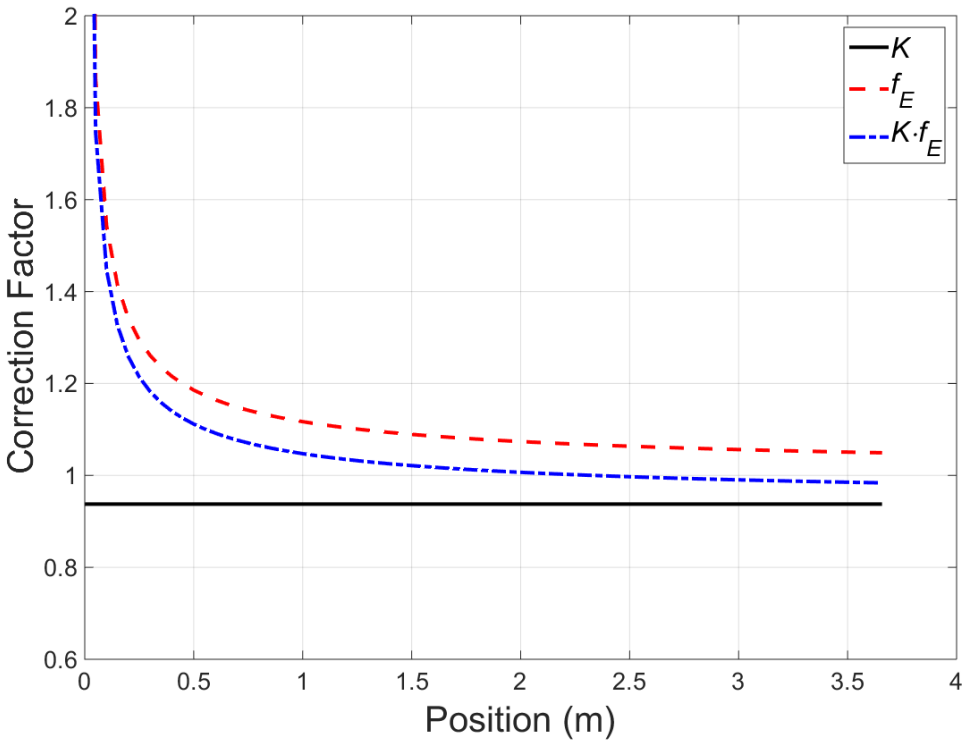

Figure 43. Values of the correction factors implemented into Aria for entrance effects and the film coefficient

To reiterate, the largest differences in the temperature between the two simulations occurred at the entrance of the annulus. This was again explained by the inability of the empirical HTC correlation used here to model thermally developing flow and would be improved with the inclusion of f_E in the HTC correlation. Last, the exit velocity profile from Aria did not significantly deviate from the average velocity profiles in Fluent. The largest differences were observed near the exit of the pipe. Changes in the velocity were more significant for annular flow compared to pipe flow as the change in air temperature was more significant along the length of the annulus. The larger thermal mass of the inner cylinder and the fact that heat transfer was occurring on more surface area resulted in the higher temperatures seen in the air.

Including both correction factors in the Gnielinski correlation annular flow may not be completely sufficient to span the difference between the Aria and Fluent. However, it should also be emphasized that different turbulence models were not explored in Fluent for annular flow. The realizable k-ε turbulence model may have been sufficient for pipe flow, but the geometry explored here possessed a significantly smaller cross sectional area where frictional effects from the walls may be more significant. While the realizable k-ε turbulence model was valid, experimental data was needed to confirm the most appropriate turbulence model to use for these comparisons.

The temperature profiles for pipe flow were also compared with the addition of a volumetric heat source on the outer pipe and inner cylinder of 5×10^5

W/m^3. Again, only the results for $\dot{m}$ = 0.65 kg/s were provided in the following four figures. However, a similar behavior in the temperature and velocity profiles was observed with all three mass flow rates.

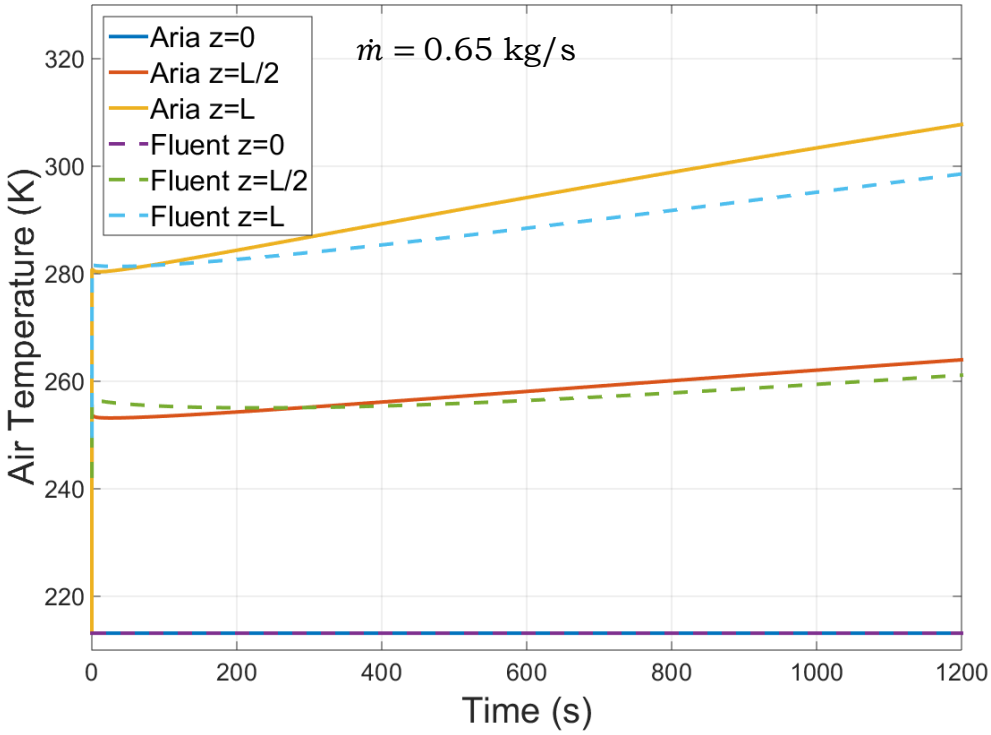

Figure 44. Air temperature profiles with time for ṁ = 0.65 kg/s at different axial locations with a volumetric source of 5×10^5 W/m^3

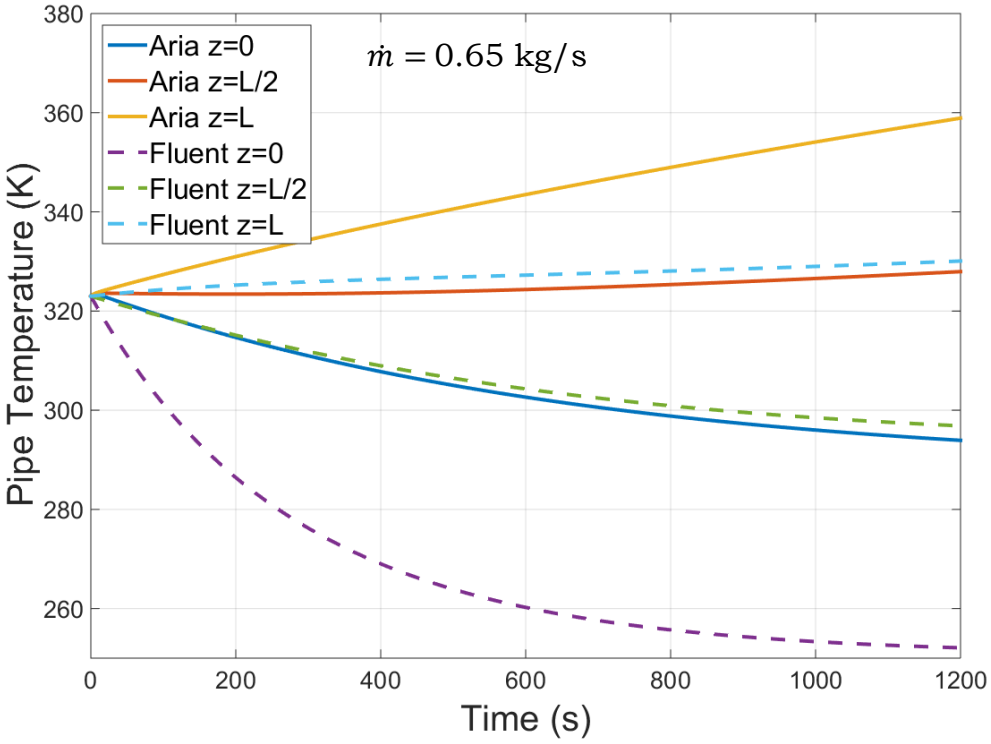

Figure 45. Exterior pipe temperature with time for ṁ = 0.65 kg/s at different axial locations with a volumetric source of 5×10^5 W/m^3

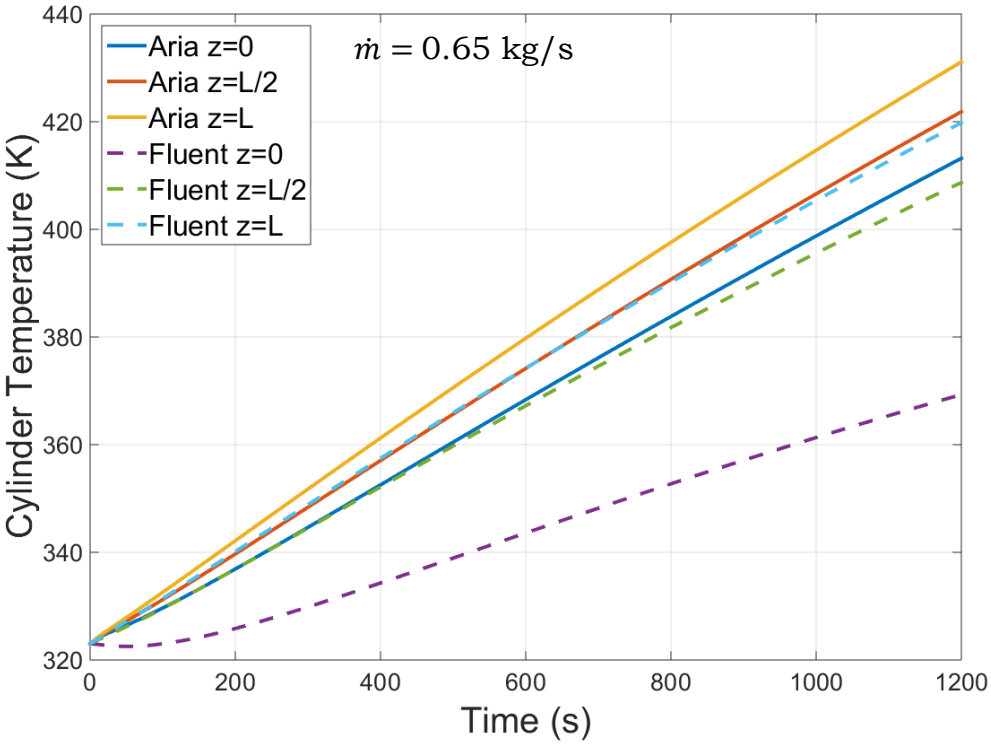

Figure 46. Inner cylinder temperature profiles with time for ṁ = 0.65 kg/s at different axial locations with a volumetric source of 5×10^5 W/m^3

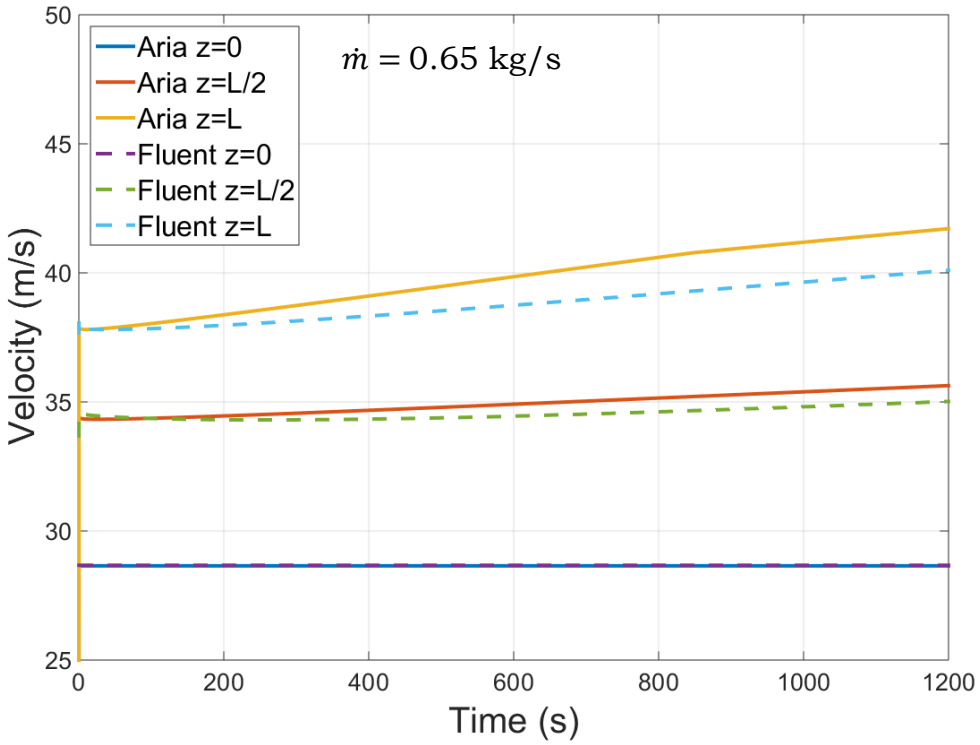

Figure 47. Velocity profiles with time for ṁ = 0.65 kg/s at different axial locations with a volumetric source of 5×10^5 W/m^3

When a volumetric heat source was included, the overall behavior of the solutions between Aria and Fluent was similar to the behavior without a heat source. Temperatures in the pipe and cylinder showed significant deviation in the solutions from Fluent by up to ~40°C at the start of the annulus. This would again be improved with the inclusion of f_E in the HTC correlation. Temperature and velocity of the air differed by a maximum of 9°C and 1.6 m/s, respectively.

Recommendations

Based on the analysis performed in this document, the following recommendations are made to analysts when incorporating advective bar elements into thermal models in Aria. These recommendations are made for geometries that are favorable for use with advective bars where the flow may be described as unidirectional. Flows of this type include pipe flow and annular flow that were explored in this work. However, it is important to reinforce that advective bar elements are not limited to these geometries and apply to a wide variety of cases. Furthermore, subsequent verification activities are also put forward in this section as suggestions for future work.

Generally, very few bar elements in the streamwise direction are required to approach a converged solution. As observed in Figure 15 through Figure 20, the solution for the fluid and the surrounding solid does not significantly depend on the number of bar elements even when there are 8 times as many elements in the solid in the streamwise direction. As a general guideline, it is recommended to use approximately ¼ the number of bar elements as there are elements in the pipe in the flow direction. Then, the number of bar elements may be increased by a factor of two in a subsequent simulation to determine if there is an appreciable effect on the solution. If not, then the former number of bar elements may be sufficient for the given problem.

Engineering judgement is required to determine if local gradients in the solid necessitate local refinement of the bar elements in nearby locations. Only uniform bar element lengths are explored in this document, but the length of each bar element is not required to be constant. The meshing of the bar elements should be conducted such that no surface in the surrounding solid is equidistant between two bar nodes. In such cases, azimuthal variations in the mapping of bar nodes to the surrounding surfaces may occur as observed in Figure 14c. Although this anomalous behavior does not occur consistently, it should still be avoided if possible. When tetrahedral elements are used a saw tooth mapping may occur as depicted in Figure 21b.

Further verification activities on the advective bar elements include repeating many of the activities performed in this document for other relevant geometries where accurate empirical heat transfer coefficient correlations are available. Such geometries include non-circular cross sections, variable area flow, and external flow. Further order of accuracy of tests should also be performed on the advective bar elements using the method of manufactured solutions (MMS) to allow comparison with an exact solution. A formal code verification test of this kind would provide confidence that the advective bar model in its current form has been properly implemented.

Summary

A new 1D fluid flow model has been integrated into Aria to model internal fluid flow over 3D solids using advective bar elements. As this is a new capability in Aria, several verification activities have been performed and described in this document to provide further confidence that the model has been properly implemented. These activities include: a mesh resolution study to ensure solution convergence, an analysis of the mapping of bar elements to the surrounding surfaces in the 3D volume, and a comparison of solutions computed using the advective bar model with the established ANSYS Fluent® commercial CFD software package.

Geometries considered for this work include simple pipe flow and annular flow. As part of the mesh resolution study, a series of uniformly refined meshes for pipe flow were used to confirm that the temperature and velocity in the fluid and the temperature in the surrounding solid converged as the mesh resolution increased. For the mapping of nodes from the bar elements to the surrounding surfaces, several meshes that varied the number of elements in the streamwise direction were visually examined. Overall, the mapping of the bar nodes to the surrounding surfaces was performed as expected. However, meshes with nodes in the bar elements and the surrounding solid that aligned in the streamwise direction experienced irregular mapping. Ultimately, meshes in which surface mesh elements on the 3D volume are equidistant between two bar nodes should be avoided, although the solution was not significantly affected by any irregularities in the mapping.

Solutions found using the advective bar elements in Aria were compared with solutions found using Fluent. While the two simulations use different physical models, the unidirectional flow of the problems considered provided comparable solutions for the temperature and velocity of the fluid and the temperature in the solids. This provided strong evidence that a 1D flow solution is adequate for the class of flow problems of interest. Differences in the solutions were primarily a result of limitations in the empirical heat transfer coefficient correlations used in the advective bar model (*e.g.* the lack of correlations that account for entrance effects). Recent implementation of correction factors to account for entrance effects should be investigated to improve the accuracy of the model.

Appendix A—Material Properties

The following temperature-dependent material properties were used for air and stainless steel in the analysis presented in this document for both Aria and ANSYS Fluent®. The data is provided in tabular form and is linearly interpolated for temperatures between the defined values. Table 5 provides the material properties for air and Table 6 provides the material properties for 304 stainless steel.

Table 5. Material Properties for Air at 0.84 atm

T (K)	ρ (kg/m^3)	c_p (J/kg·K)	k (W/m·K)	μ (µPa·s)
100	2.987	1032	0.00934	7.11
150	1.963	1012	0.0138	10.34
200	1.466	1007	0.0181	13.25
250	1.172	1006	0.0223	15.96
300	0.976	1007	0.0263	18.46
350	0.836	1009	0.03	20.82
400	0.732	1014	0.0338	23.01
450	0.650	1021	0.0373	25.07
500	0.585	1030	0.0407	27.01
600	0.532	1051	0.0469	30.58

Table 6. Material Properties for 304 Stainless Steel

T (K)	c_p (J/kg·K)	T (K)	k (W/m·K)
100	460.0	173.15	10.89
273.15	502.4	273.15	13.40
673.15	565.2	373.15	16.33
1000	611.0	773.15	21.77
1200	640.0	973.15	25.96
1500	682.0	3500	25.96

Appendix B—Validation Procedure

To further support the implementation of the advective bar elements into Aria, a procedure to validate the model is provided here. The purpose of validation is to provide additional confidence to analysts that the advective bar model produces physically realistic solutions. While the previous comparison to the commercial CFD code ANSYS Fluent® provides some confidence that the model is realistic given Fluent's standing in the fluid sciences community, a more rigorous comparison to experimental results is required.

One approach to validating the advective bar is to utilize existing experimental data in the literature for similar geometries to those that have already been investigated in this document (*i.e.* pipe flow and annular flow). Therefore, an extensive literature review would be performed to find suitable candidate problems for comparison. Measurements from these experiments would be compared to solutions from simulations of the candidate geometry in Aria using the advective bar model. The advantage of this approach is that geometries could be evaluated quickly without the time and resources invested in constructing and performing an experiment. The downside to this approach is that the suitable candidates need to possess all the necessary detail in the experimental setup and procedure in the literature. Small details unintentionally omitted may need to be assumed if sufficient information is not provided.

An alternative approach is to construct a low-cost experiment that is specifically tailored to producing the necessary experimental data needed to validate the advective bar model. This would ensure that all the information is present to properly compare with the model. In addition, the most relevant geometry and experimental conditions can be used that would be applicable to thermal analysis already being performed at Sandia. For completeness, an experimental setup is proposed here that would be sufficient for validating the advective bar elements.

The following experiment, depicted in Figure 48, is proposed to provide validation data for transient flow. This experiment is designed with the following guidelines: that it can be setup and performed quickly, it is inexpensive and requires minimal machining, and it has a small footprint. The experiment is performed as a simplified and scaled experiment of the test in Reference 1, where matching the Reynolds number *Re* is sufficient to gather the necessary thermal data reducing the need for large mass flow rates.

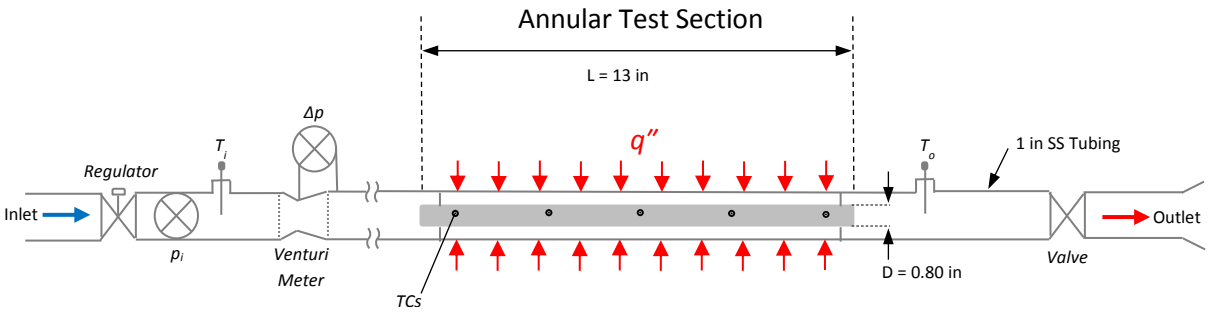

Figure 48. Schematic of the Proposed Experiment

Compressed air from a building supply is used as the working fluid at room temperature. Air flows through a pressure regulator to set the inlet pressure of the flow and then through a Venturi meter to measure the volumetric flow rate. Pressure and temperature are measured at the inlet to the Venturi meter to measure the fluid density and ultimately the mass flow rate. The fluid then flows to the annular test section after sufficient distance to ensure a fully developed profile. The outer annulus wall of the test section is made from thin walled 1" OD stainless steel tubing to ensure axial conduction is negligible. The outer annulus wall of the tubing is wrapped in a blanket heater providing heat fluxes q'' up to 30 kW/m^2 to pass to the fluid for the duration of the experiment. The heat is then convected to the inner cylinder of the test section through the air where the temperature is measured along the length of the annulus with embedded thermocouples at a predefined depth. The diameter D = 0.80 in (2.032 cm) and length L = 13 in (0.3302 m) of the inner cylinder is sufficient to provide similar conditions and Re encountered in Reference 1 ($Re \approx 1.1\times10^5$). However, achieving these Re depends on the capability of the building air supply providing steady mass flow rates $\dot{m} \approx 0.07$ kg/s. For this mass flow rate and cross sectional area, an inlet pressure $P_i > 50$ psig (344 kPa gauge) is needed to ensure that Mach number M is sufficiently low to assume incompressible flow ($M < 0.34$). Pressure drop across the test section is expected to be ~10 psi. The inlet and outlet temperatures are measured with RTDs, which can also be used to confirm the heat flux from the blanket heater if the experiment is sufficiently insulated. A valve at the exit of the test section is used to control the mass flow rate. Temperatures in the inner cylinder are then compared with the solutions provided by the advective bar elements in Aria to validate the model. Air temperature along the length of the test section can also be measured with thermocouples for more validation data.

Ports will need to be placed along the length of the annulus outer wall to allow thermocouples to enter the test section. This method will provide a simple approach for assembling the annulus and embedding the thermocouples. The inner cylinder of the annulus is constructed of C36000 free machining brass for easy drilling of the thermocouple holes. Other low cost materials could also

be used provided they have accurate thermal property data available. Overall, the majority of the cost for the experiment setup resides in the instrumentation. Machining is limited to parts in the test section for thermocouple holes and ports, spacers for the inner cylinder, and the diameter of the inner cylinder, which are all very simple modifications. All piping can be constructed with off-the-shelf metal tube and tube fittings.

For the experiment in its present form described above, increasing the incident heat flux on the outer surface of the pipe may be required to achieve a sufficient temperature increase on the inner cylinder. That is, a sufficient temperature increase on the cylinder is required to assuredly exceed the uncertainty in the thermocouples used. However, it may prove difficult to find higher heater power in off-the-shelf products specifically tailored for the geometry specified. If a heater with a larger power cannot be easily sourced, then the test section length may be increased to achieve more power provided the experiment has significant floor space. The test section could also be mounted vertically to decrease its footprint (at these *Re*, buoyancy driven flow is negligible). Another approach would be to scale the test section diameter to allow more surface area on the outside of the pipe; however this increases the required mass flow rate to achieve $Re \approx 1.1\times10^5$. Other considerations for the heater include the need to allow the ports on the outside of the annulus for the instrumentation. If none of the previously stated options are sufficient to achieve the desired temperatures on the inner cylinder, then lower *Re* will need to be considered. Alternatively, the heat source can be placed on the inner cylinder of the annulus using custom polyimide heaters (see Reference 1) to achieve higher temperatures. This approach may require that the heaters themselves are included in the model as they will introduce additional uncertainty in the use of appropriate empirical HTC correlations.

Given that the accuracy of the advective bar capability is sensitive to the empirical HTC correlation, it is important to determine the best practices for the type of flow being modeled. At present, the best empirical HTC correlations for annular flow implemented into Aria are the Gnielinski correlations (Reference 19). These correlations were compiled from a number of sources for annular flow with heat transfer occurring on the inner cylinder or the outer wall. The data in this experiment can also be used to provide the necessary guidance for modeling annular flow with these correlations, a very common and relevant geometry and one already used with advective bar elements. For example, the need and validity of additional correction factors to account for entrance effects can be evaluated.

Distribution:

1	MS-0346	01514	D. Dobranich
1	MS-0825	01544	A. Hetzler
1	MS-0825	01514	B. Mills

Electronic copies only:

1	MS-0346	01514	D. Dobranich
1	MS-0346	01514	L. Phinney
1	MS-0386	02159	A. Subbiah
1	MS-0386	02159	V. Ragsdale
1	MS-0825	01514	B. Mills
1	MS-0825	01544	A. Hetzler
1	MS-0828	01544	K. Dowding
1	MS-0828	01514	H. Silva
1	MS-0828	01514	J. Yuan
1	MS-0836	01541	T. Okusanya
1	MS-0836	01541	S. Subia
1	MS-0836	01514	R. Hogan Jr.
1	MS-0836	01514	M. Larsen
1	MS-0836	01514	N. Francis
1	MS-0836	01514	J. Shelton
1	MS-0836	01514	M. Pilch
1	MS-0840	01514	J. Tencer
1	MS-1135	01532	T. Blanchat
1	MS-0899		Technical Library, 9536 (electronic copy)


Sandia National Laboratories